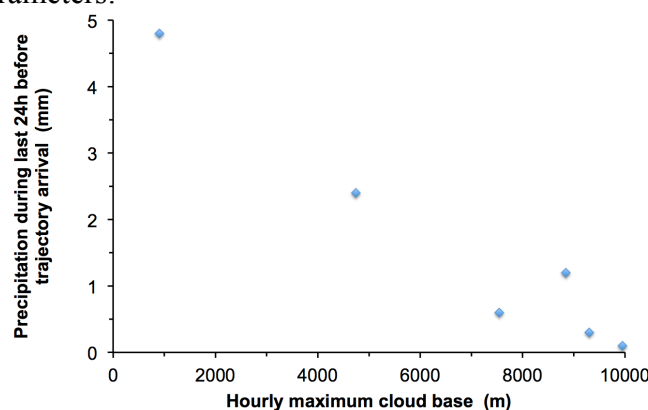Major comments:

1. We added the suggested references to the discussion of growth rates.

2. The possibility that sporadic anthropogenic emissions were interpreted as NPF events cannot be excluded completely. However, there are a number of facts arguing strongly against this possibility leading to serious misinterpretation of the data:
   a) Location and operation of the Mt. Zeppelin station exclude local contamination to a very large extent.
   b) Manual inspection of the time series by one of the co-authors (PT) further reduced the risk of contaminated data.
   c) The temporal evolution of MEV events, i.e. concurrent and sustained concentration increases at several particle sizes below 60 nm does not correspond to a typical passage of stack emissions from a large combustion source, (Ogren and Heintzenberg, 1990). Instead, it looks very much like MEV events observed under even stricter constraints on local or regional sources of contamination on icebreaker Oden in the central pack ice area, (Karl et al., 2013), and, according to reviewer #2 also looks similar to nocturnal NPF-events in Australian forests.

3. The hypothesis of gel-forming phytoplankton contributing to NPF has been elaborated extensively in the introduction, supported by a large number of references (Karl et al., 2013; Karl et al., 2012; Orellana et al., 2011; Leck and Bigg, 2010; Leck and Bigg, 2005a, b, c; Leck et al., 2004). The data available to date do not allow statements about the dominance of this hypothesized mechanism.

4. We added the following text to the section introducing the model-calculated meteorological parameters: "We emphasize that their accuracy depends on the quality of the meteorological model inside HYSPLIT4 and on the accuracy and representativeness of the meteorological fields utilized by the model. Of the local meteorological record the frequently recorded air temperature was considered the most reliable and thus explored in a comparison of trajectory calculated and modeled local meteorological data. When comparing the 42600 contiguous hourly records from 2008-01-01 until 2012-11-10 the average ratio of measured and calculated temperatures is 0.98, with a coefficient of determination of 0.96."
   The ceilometer data did not include precipitation. However, the statistics below might be able to reduce the reviewer's doubts about the quality of the model-calculated meteorological parameters:

Minor comments:

Comment	Response
Line 29	Changed as suggested
Line 30	Yes, the sentence now begins with "The occurrence of NPF-events appears to be somewhat sensitive…"
Line 34	Changed as suggested
Introduction	Building on a short quantification of the dataset the last paragraph of the introduction does just what the reviewer requests, i.e. describes the aim of the study. Thus, we would like to keep this paragraph where it stands.
Solar flux is not described in Database, but used in data analysis.	All utilized parameters were described in Table 1. To clarify the text further we added to the caption of Table 1: All parameter explanations starting with "Trajectory" refer to parameters calculated by HYSPLIT4 at each trajectory step. Also, we added the sentence The utilized model parameters are listed in Table 1 in the database section after introducing the model- calculated parameters.
Line 200	Changed as suggested
Line 217	Changed as suggested
Line 235	Changed as suggested, albeit citing Stohl (1998).
Line 249	Changed as suggested
Line 255	Changed as suggested
Line 258	Changed as suggested
Line 275	Changed as suggested
Line 277	We added the sentence "The products of the photochemical oxidation of DMS the ratio MSA/ $nssSO_4^{2-}$ show a temperature dependence (Bates et al., 1990), favoring MSA in the cold Arctic environment (Karl et al., 2007)."
Line 438	We do not feel that the suggested change would improve the readability of the paper and appeal to the editor to disregard this suggestion
Line 509	No, as stated on lines 464 to 466: "Besides these common characteristic lengths individual fixed thresholds were chosen and discussed below for each approach in order to generate at least 200 unique events per approach, (see Table 2). An additional column in Table 2 now shows the fraction of the total number of hours covered by unique events of the three types.

Line 654	Corrected
Line 755	"Arctic stratus" is a generally accepted term in the Arctic literature since at least 1976. We prefer to maintain the wording as is.
Line 764	Yes, however, the molar ratio of MSA to nssSO4 could be used as a proxy for sorting
Line 787	Changed as suggested
Line 827	Changed as suggested
Line 847	Changed as suggested
Line 868	We disagree because of (as stated in the paper) "the relatively small daily variations in solar elevations"
Conclusions are too long and descriptive	To make the title of this section more appropriate it now reads "Summary and conclusion"
Line 912	"change in" as stated
Figure 6	Yes, information added to the captions of Figs. 6, 9, and 10.

Literature

Bates, T. S., Johnson, J. E., Quinn, P. K., Goldan, P. D., Kuster, W. C., Covert, D. C., and Hahn, C. J.: The biogeochemical sulfur cycle in the marine boundary layer over the Northeast Pacific Ocean, J. Atmos. Chem., 10, 59-81, 1990.

Karl, M., Gross, A., Leck, C., and Pirjola, L.: Intercomparison of dimethylsulfide oxidation mechanisms for the marine boundary layer: Gaseous and particulate sulfur constituents, J. Geophys. Res., 112, D15304, 10.1029/2006JD007914, 2007.

Karl, M., Leck, C., Gross, A., and Pirjola, L.: A Study of New Particle Formation in the Marine Boundary Layer Over the Central Arctic Ocean using a Flexible Multicomponent Aerosol Dynamic Model, Tellus, 64B, doi:http://dx.doi.org/10.3402/tellusb.v3464i3400.17158, 2012.

Karl, M., Leck, C., Coz, E., and Heintzenberg, J.: Marine nanogels as a source of atmospheric nanoparticles in the high Arctic, Geophys. Res. Lett., 40, 3738–3743, DOI: 10.1002/grl.50661, 2013.

Leck, C., Tjernström, M., Matrai, P., Swietlicki, E., and Bigg, K.: Can marine micro-organisms influence melting of the Arctic pack ice?, EOS, 85, 25-36, 2004.

Leck, C., and Bigg, E. K.: Evolution of the marine aerosol - A new perspective, Geophys. Res. Lett., 32, doi:10.1029/2005GL023651, 2005a.

Leck, C., and Bigg, E. K.: Source and evolution of the marine aerosol - A new perspective, Geophys. Res. Lett., 32, L19803, doi:19810.11029/12005GL023651, 2005b.

Leck, C., and Bigg, E. K.: Biogenic particles in the surface microlayer and overlaying atmosphere in the central Arctic Ocean during summer, Tellus, 57B, 305–316, 2005c.

Leck, C., and Bigg, E. K.: New particle formation of marine biological origin, Aerosol Sci. Technol., 44, 570-577, 2010.

Ogren, J. A., and Heintzenberg, J.: Parametric aerosol sampling at low concentration levels, Department of Meteorology, Stockholm UniversityAA-1, 1990.

Orellana, M. V., Matrai, P. A., Leck, C., Rauschenberg, C. D., Lee, A. M., and Coz, E.: Marine microgels as a source of cloud condensation nuclei in the high Arctic, PNAS, 108, 13612–13617, 2011.

Stohl, A.: Computations, accuracy and applications of trajectories - A review and bibliography, Atmos. Environ., 32, 947-966, 1998.

Major comments:

1. We politely ask to disagree with reviewer #2. In section 3.2 we did list and discuss the growth rates that the reviewer is missing and compare them to other Arctic and subarctic results. After suggestions of reviewer #1 this discussion is widened to include growth rates measured over the North Atlantic.

2. Assuming that reviewer # 2 means global radiation with the acronym GR and condensation sink with the acronym CS we fail to see substantial additional value in a scatter plot of formation rates at 10 nm rates versus CS/GR, in particular since much of the data set does not include particles smaller than 10 nm.

3. We feel comfortable with our definition of PCT-events, (which reviewer #2 did not object to). From our data one cannot make any statements about a "lack of growth" because we have no information on any growth processes that occurred before the particles reached diameters that we could sense with our instruments.

4. We are most grateful for the information about NPF-events in Australian Eucalyptus forests comparable to our MEV-events and included three related "Suni papers" in our discussion of MEV-events with the text "The concurrent appearance of high concentrations at many particle sizes below 60 nm resembles the nocturnal NPF-events analyzed by Suni et al. (2008) in the Australian Eucalyptus forest and simulated in subsequent chamber experiments (Ristovski et al., 2010; Junninen et al., 2008). We emphasize though that the condensing vapors in the Australian NPF-events originating from terrestrial biogenic emission are quite different from the polymer gels implicated in the Arctic MEV-events and originating from the surface microlayer of the ocean."

Minor comment:

We updated the address of Peter Tunved

Literature

Bates, T. S., Johnson, J. E., Quinn, P. K., Goldan, P. D., Kuster, W. C., Covert, D. C., and Hahn, C. J.: The biogeochemical sulfur cycle in the marine boundary layer over the Northeast Pacific Ocean, J. Atmos. Chem., 10, 59-81, 1990.
Junninen, H., Hulkkonen, M., Riipinen, I., Nieminen, T., Hirsikko, A., Suni, T., Boy, M., Lee, S.-H., Vana, M., Tammet, H., Kerminen, V.-M., and Kulmala, M.: Observations on nocturnal growth of atmospheric clusters, Tellus B, 60, 365-371, 2008.
Karl, M., Gross, A., Leck, C., and Pirjola, L.: Intercomparison of dimethylsulfide oxidation mechanisms for the marine boundary layer: Gaseous and particulate sulfur constituents, J. Geophys. Res., 112, D15304, 10.1029/2006JD007914, 2007.
Karl, M., Leck, C., Gross, A., and Pirjola, L.: A Study of New Particle Formation in the Marine Boundary Layer Over the Central Arctic Ocean using a Flexible Multicomponent Aerosol Dynamic Model, Tellus, 64B, doi:http://dx.doi.org/10.3402/tellusb.v3464i3400.17158, 2012.
Karl, M., Leck, C., Coz, E., and Heintzenberg, J.: Marine nanogels as a source of atmospheric nanoparticles in the high Arctic, Geophys. Res. Lett., 40, 3738–3743, DOI: 10.1002/grl.50661, 2013.

Leck, C., Tjernström, M., Matrai, P., Swietlicki, E., and Bigg, K.: Can marine micro-organisms influence melting of the Arctic pack ice?, EOS, 85, 25-36, 2004.

Leck, C., and Bigg, E. K.: Evolution of the marine aerosol - A new perspective, Geophys. Res. Lett., 32, doi:10.1029/2005GL023651, 2005a.

Leck, C., and Bigg, E. K.: Source and evolution of the marine aerosol - A new perspective, Geophys. Res. Lett., 32, L19803, doi:19810.11029/12005GL023651, 2005b.

Leck, C., and Bigg, E. K.: Biogenic particles in the surface microlayer and overlaying atmosphere in the central Arctic Ocean during summer, Tellus, 57B, 305–316, 2005c.

Leck, C., and Bigg, E. K.: New particle formation of marine biological origin, Aerosol Sci. Technol., 44, 570-577, 2010.

Ogren, J. A., and Heintzenberg, J.: Parametric aerosol sampling at low concentration levels, Department of Meteorology, Stockholm UniversityAA-1, 1990.

Orellana, M. V., Matrai, P. A., Leck, C., Rauschenberg, C. D., Lee, A. M., and Coz, E.: Marine microgels as a source of cloud condensation nuclei in the high Arctic, PNAS, 108, 13612–13617, 2011.

Ristovski, Z. D., Suni, T., Kulmala, M., Boy, M., Meyer, N. K., Duplissy, J., Turnipseed, A., Morawska, L., and Baltensperger, U.: The role of sulphates and organic vapours in growth of newly formed particles in a eucalypt forest, Atmos. Chem. Phys., 10, 2919-2926, 10.5194/acp-10-2919-2010, 2010.

Stohl, A.: Computations, accuracy and applications of trajectories - A review and bibliography, Atmos. Environ., 32, 947-966, 1998.

Suni, T., Kulmala, M., Hirsikko, A., Bergman, T., Laakso, L., Aalto, P. P., Leuning, R., Cleugh, H., Zegelin, S., Hughes, D., van Gorsel, E., Kitchen, M., Vana, M., Hõrrak, U., Mirme, S., Mirme, A., Sevanto, S., Twining, J., and Tadros, C.: Formation and characteristics of ions and charged aerosol particles in a native Australian Eucalypt forest, Atmos. Chem. Phys., 8, 129-139, 10.5194/acp-8-129-2008, 2008.

1

2

3

New particle formation in the Svalbard region 2006 - 2015

5

Jost Heintzenberg[1], Peter Tunved[2], Martí Galí[3], and Caroline Leck[4]

7

8

9   1:   Leibniz Institute for Tropospheric Research (TROPOS), Permoserstr. 15, 04318 Leipzig,

10   Germany

11   2:   Department of Environmental Science and Analytical Chemistry (ACES), Stockholm

12   University, 10691 Stockholm, Sweden

13   3:   Takuvik Joint International Laboratory & Québec-Océan, Université Laval, G1V 0A6

14   Québec, Canada

15   4:   Department of Meteorology, Stockholm University (MISU), 10691 Stockholm, Sweden

16

20   Abstract

21

22   Events of new particle formation, (NPF), were analyzed in a ten-year data set of hourly

23   particle size distributions recorded on Mt. Zeppelin, Spitsbergen, Svalbard. Three different

24   types of NPF-events were identified through objective search algorithms. The first and

25   simplest algorithm utilizes short-term increases in particle concentrations below 25 nm,

26   (PCT-events). The second one builds on the growth of the sub-50 nm diameter-median,

27   (DGR-events), and is most closely related to the classical "banana-type" of events. The third

28   and most complex, so-called multiple-size approach to identifying NPF-events builds on a

29   hypothesis suggesting the concurrent production of polymer gel particles at several sizes

30   below about 60 nm, (MEV-events).

31   As a first and general conclusion we can state that NPF-events are a summer phenomenon

32   and not related to Arctic haze, which is a late winter-to-early spring feature. The occurrence

33   of NPF-events appears to be somewhat sensitive to the available data on precipitation. The

34   seasonal distribution of solar flux suggests some photochemical control that may affect

35   marine biological processes generating particle precursors and/or atmospheric photochemical

36   processes that generate condensable vapors from precursor gases. Notable, the seasonal

37   distribution of the biogenic methanesulfonate, (MSA), follows that of the solar flux although

38   it peaks before the maxima in NPF-occurrence.

39   A host of ancillary data and findings point to varying and rather complex marine biological

40   source processes. The potential source regions for all types of new particle formation appear

41   to be restricted to the marginal ice and open water areas between Northeastern Greenland and

42   Eastern Svalbard. Depending on conditions yet to be clarified new particle formation may

43   become visible as short bursts of particles around 20 nm, (PCT-events), longer events

44   involving condensation growth, (DGR-events), or extended events with elevated

45   concentrations of particles at several sizes below 100 nm, (MEV-events). The seasonal

rev. 2017-2-18 10:48
Gelöscht: event.

rev. 2017-2-18 10:48
Gelöscht: appear

rev. 2017-2-18 10:48
Gelöscht: Whereas

49   distribution of NPF-events peaks later than that of MSA and, DGR and in particular of MEV-

50   events reach into late summer and early fall with much open, warm, and biologically active

51   waters around Svalbard. Consequently, a simple model to describe the seasonal distribution

52   of the total number of NPF-events can be based on solar flux, and sea surface temperature,

53   representing environmental conditions for marine biological activity, and condensation sink,

54   controlling the balance between new particle nucleation and their condensational growth.

55   Based on the sparse knowledge about the seasonal cycle of gel-forming marine

56   microorganisms and their controlling factors we hypothesize that the seasonal distribution of

57   DGR and more so MEV-events reflect the seasonal cycle of the gel-forming phytoplankton.

58

59

60   **1. Introduction**

61

62   In the late 1970ies and early 1980ies the interest in the Arctic atmospheric aerosol widened

63   from the well-identified winter phenomenon of Arctic haze (Rahn and Shaw, 1977;

64   Heintzenberg and Leck, 1994) to summer conditions in this northernmost remote region. In

65   the pristine Arctic summer air the so-called background aerosol (Junge, 1963) was expected

66   to be most clearly visible, far away from the northern hemispheric anthropogenic emission

67   centers at lower latitudes. Episodic and localized occurrences of high concentrations of

68   ultrafine particles, (here defined as particles with diameters < 100 nm), in the summer Arctic

69   were explained by rare import of polluted air from lower latitudes (Flyger and Heidam, 1978;

70   Heintzenberg and Larssen, 1983) or hypothetical anthropogenic sources in the Arctic

71   (Jaenicke and Schütz, 1982).

72   With the advent of sensitive condensation nuclei counters (Agarwal and Sem, 1980) and

73   differential mobility analyzers (Knutson and Whitby, 1975b, a) more details became visible in

74   the Arctic sub-micrometer aerosol. High numbers of ultrafine particles were observed in

75   connection with fog passages (Lannefors et al., 1983) and chemical aerosol information

76   indicated a regional – possibly biogenic – particle sources in the summer Arctic

77   (Heintzenberg, 1989). The high molar ratios of methane sulfonate, (MSA), to non-sea salt

78   sulfate, (nssSO$_4^{2-}$), of 0.28 in the Arctic summer aerosol found by Heintzenberg and Leck

79   (1994) substantiated the biogenic source of the particles.

80   The establishment of long-term Arctic aerosol monitoring at the fringes of the pack ice in

81   Alaska (e.g., Polissar et al., 1999), Canada (e.g., Norman et al., 1999; Willis et al., 2016), and

82   on Spitsbergen (e.g., Tunved et al., 2013) revealed more details of potential sources of the

83   summer aerosol, in particular their connection to the marine biosphere in the Arctic. The

84   unique series of systematic aerosol studies in the central Arctic north of 80°N onboard the

85   Swedish icebreaker *Oden* in 1996 led to the formulation of a new hypothesis concerning a

rev. 2017-2-18 10:48
Gelöscht: (Knutson and Whitby, 1975a, b)

rev. 2017-2-18 10:48
Gelöscht: (e.g., Tunved et al., 2013)

88   specific process of marine biogenic particle formation (Leck and Bigg, 1999). The marine

89   biogenic particles involved behaved as polymer gels and originated in the surface microlayer

90   (SML) of the ocean, (Orellana et al., 2011b), from the activity of sea-ice algae,

91   phytoplankton and, perhaps, bacteria. The new particle events were reported to occur as

92   simultaneous enhancement of particle number concentrations in the whole size-range below

93   50 nm, and not with the prototypical "banana growth" (Kulmala et al., 2004). Two more

94   *Oden* cruises in 2001 and 2008 yielded results that were partly contradicting (Held et al.,

95   2011b; Held et al., 2011a), partly supporting the SML hypothesis (Leck et al., 2013; Karl et

96   al., 2013; Orellana et al., 2011b; Leck and Bigg, 2010). The synopsis of the results of four

97   *Oden* cruises of Heintzenberg et al. (2015) identified geographic regions of new particle

98   formation (NPF) in the inner Arctic while stressing the importance of recent open water and

99   related biological activity in the sea in transects by air masses with new particle formation

100   over the central Arctic.

101   Two years of aerosol size distributions from Mt. Zeppelin, Spitsbergen and Alert, both

102   located at the fringes of the central pack ice, were analyzed by Croft et al. (2016a) with a

103   global aerosol geophysics model. They discuss classical new-particle nucleation, coagulation

104   scavenging in clouds, scavenging by precipitation, and transport in order to explain the annual

105   cycle of the Arctic aerosol. Croft et al. (2016a) find two seasonal maxima in their modeled

106   particle nucleation rates, one in March, and one in July. In spring, their simulated NPF occurs

107   mainly in the free troposphere, whereas in summer, it occurs also in the planetary boundary

108   layer. More recently, Croft et al. (2016b) state that ammonia from seabird-colony guano is a

109   key factor contributing to bursts of newly formed particles, which are observed every summer

110   in the near-surface atmosphere, at least at Alert, Nunavut, Canada. Earlier, the results of

111   studies with another global aerosol model by Browse et al. (2014) suggested that the potential

112   increase in NPF in the Arctic with potential increases in cloud condensation nuclei is

113 compensated by wet scavenging. They also state that scavenging by pre-existing large

114 particles suppresses NPF-events.

115 Based on three years of data from the two Arctic sites Thule and Ny-Ålesund (gruvebadet)

116 Becagli et al. (2016) examined the sources and environmental factors controlling the

117 biological aerosol component MSA. Their analysis included satellite-derived Chlorophyll-*a*

118 (an indicator of phytoplankton biomass), oceanic phytoplankton primary productivity, (PPP),

119 and sea ice. Whereas they found good correlations between MSA, PPP and sea ice, (the latter

120 two being closely related), their data did not allow any statements on NPF processes.

121 To date the longest record of sub-micrometer number-size distributions of the Arctic

122 aerosol down to 5 nm particle diameter and below has been accumulated on Mt. Zeppelin,

123 Spitsbergen (Tunved et al., 2013; Heintzenberg and Leck, 1994). For the ten years from 2006

124 through 2015 a total of 63936 quality-controlled hours of aerosol data are available, i.e.

125 during 73% of all hours of the ten years. In the present study we exploit this formidable data

126 set in a search for processes forming new particles. An important first step in this work was

127 formulating completely objective criteria for the identification of events. In the relatively

128 clean Arctic environment we do not expect the classical nucleation and growth events as

129 frequently observed over the continents, (cf. Kulmala et al., 2004), to dominate. Thus, we

130 refrained from applying the objective search algorithm formulated by Heintzenberg et al.,

131 (2007) for this "Banana-type" of events. Instead we formulated new objective search

132 algorithms allowing several potential types of new particle formation events or formation

133 processes. With a host of complementary atmospheric and surface physical, chemical, and

134 biological information a large number of NPF-events identified with these algorithms will be

135 analyzed in the following chapters.

136

137

138

139   **2. Database**

140

141   The Mt. Zeppelin observatory

142

143   Situated at the top of Mt Zeppelin, Svalbard (78° 56'N, 11° 53'E), the Zeppelin observatory

144   offers a unique possibility to study the characteristic features of Arctic atmospheric

145   constituents such as trace gases and aerosol particles. At a height of 474 m a.s.l. the station is

146   located near the top of the local planetary boundary layer and represents remote Arctic

147   conditions. The closest source of pollution, the small community of Ny-Ålesund, is located

148   ~2   km   north   of   the   station

149   (http://www.esrl.noaa.gov/psd/iasoa/sites/default/files/stations/nyalesund/nyalesund_site.jpg).

150   However, the elevation difference and typical wind patterns largely prevent pollution from

151   nearby sources to reach the Zeppelin Observatory. The dominating wind pattern is east-

152   southeast katabatic flow from Kongsvegen glacier or from northwesterly directions as

153   channeled by the Kongsfjord (Beine et al., 2001; Heintzenberg et al., 1983). The station itself

154   was initially established in 1991, and is owned by the Norwegian Polar Research Institute

155   (NP). The Norwegian Institute for Air Research (NILU) is responsible for the coordination of

156   the scientific program.

157

158

159   **2.1   Physical aerosol data**

160

161   After a period of continuous aerosol measurements by the Department of Meteorology,

162   Stockholm University in the early 1990ties, (Heintzenberg and Leck, 1994), the Department

163   of Analytical Chemistry and Environmental Science, Stockholm University, initialized

164   observations of the aerosol number size distribution in mid-2000. Originally, the system

consisted of a single differential mobility analyzer system, (DMPS), consisting of a medium-size Hauke-type differential mobility analyzer, (DMA), together with a TSI 3760 condensation particle counter, covering diameters between 20 and ~500nm. From 2006 on the particle size range was widened covering particle sizes between 10 and 790 nm. In 2005, the rain-cover over the inlet was replaced. Initially, the instrument inlet was of a PM10 type, removing particles or hydrometeors with diameters >10 μm from the sampled air stream. During a substantial renewal of the Stockholm University equipment in 2010-2011, both inlet and DMPS system were replaced.

Since then, the DMPS-system utilizes a custom-built twin DMA-setup comprising one Vienna-type medium DMA coupled to a TSI CPC 3010 covering sizes between 25-800 nm and a Vienna-type long DMA coupled with at TSI CPC 3772 covering sizes between 5-60 nm. The size distributions from the two systems are harmonized on a common size grid and then merged. Both systems use a closed-loop flow setup. The current inlet hat is of whole air type, complying with EUSAAR[1] standard for high altitude or Arctic sampling conditions. In the current setup, the inlet is operated with a flow of ca. 100 liters per minute, (lpm). Laminar flow conditions apply throughout the sampling lines. Outside of the station, the inlet temperature is kept above 0°C using active heating. Inside the station the temperature increases gradually to room temperature (maximum temperature reaches ca. 25 °C, but remains typically around 20°C). Relative humidity, (RH) and temperature are internally monitored and measurements are maintained at dry conditions with RH < 30%. The system is regularly checked with latex spheres and flow controls. The recorded data are manually screened and crosschecked with other available observation as in Tunved et al. (2013). If inconsistencies were found between the different datasets, further investigation was

---

[1] EUSAAR (European Supersites for Atmospheric Aerosol Research) is an EU-funded I3 (Integrated Infrastructures Initiatives) project carried out in the FP6 framework of the specific research and technological development gram "Structuring the European Research Area - Support for Research Infrastructures", (http://www.eusaar.net/).

189   performed to exclude data that were identified as affected by instrumental errors. Using the

190   instrumental logbook, periods of local activity potentially influencing the sampling were also

191   excluded from the dataset. During the years 2006 – 2010 no particles below ten nanometers

192   in diameter were recorded. From 2011 on four more diameter bins down to 5 nm were

193   included and a different diameter array was utilized. To allow for a synopsis of all years all

194   size distributions were interpolated on the pre-2011 diameter array and all integrals of the size

195   distribution over particle diameter were taken over the joint diameter range 10 to 631 nm. For

196   the pre-2011 years the data at the four size channels below 10 nm were flagged as missing.

197   However, whenever results cover the complete time series the resulting number

198   concentrations in the four first channels covering the years 2011 – 2015 are carried along.

199   For the identification of NPF in terms of particle growth the parameter D50 in nanometer

200   was calculated as the number median diameter of particles smaller than 50 nm but larger than

201   10 nm, i.e. 50% of all particles below that size are smaller than D50. Besides this parameter

202   Table 1 lists nine integral particle parameters, which are utilized in the NPF-search

203   approaches or in the interpretation of results. These aerosol parameters quantify total particle

204   number, (NTO), and particle numbers in sub-ranges of the number size distribution such as

205   N25, quantifying the total number of particles between ten and 25 nm.

206   Following the concept developed by Pirjola et al., (1999), and Kulmala et al., (2001) we

207   calculated the condensation sink, (CS, s^{-1}), as a parameter with which the probability of new

208   particle formation from the gas phase and the necessary amount of condensable vapor can be

209   estimated. We utilized number size distributions, pressure and temperature taken from our

210   database for this calculation.

211

212

213

214

217 **2.2 Chemical aerosol data**

218

219 For the interpretation of NPF-events we employed chemical information derived from the

220 analyses of high volume particle samples taken by the Norwegian Institute for Air research,

221 (NILU). A high volume sampler (PM10) was used to collect samples for a quantitative

222 determination of sodium, (Na^+), sulfate, (SO_4^{2-}) and MSA (CH_3SOO^-). The sampler collected

223 material for analysis in one to three days. Blank samples were obtained by mounting the

224 glass fiber filters at the sampling site with the same sampling period but without air passing

225 through. Na^+ and SO_4^2 were analyzed by NILU and have been downloaded for the present

226 study from the EBAS database (http://ebas.nilu.no), which list details about the sampling

227 technique and the sampling protocol. Nss SO_4^{2-} was determined from total sulfate correcting

228 for sea salt sulfate as $0.25xNa^+$ (Keene et al., 1986).

229   MSA was analyzed at the laboratory of the Department of Meteorology, Stockholm

230 University. To allow for subsequent chemical determinations the ambient samples and blanks

231 were carefully handled in a glove box (free from particles, sulfur dioxide and ammonia). At

232 the time of the chemical analyses, still in the glove box, the substrates were extracted (in

233 centrifuge tubes) with 60 cm^3 deionized water (Millipore Alpha-Q, conductivity 18 MΩcm).

234 The extracts were thereafter analyzed for weak anions by chemically suppressed ion

235 chromatography (IC, Dionex ICS-2000) using Dionex AG11/AS11 columns. In order to trap

236 carbonates and other ionic contaminants a Dionex ATC-1 column was used before the

237 injection valve. The injection volume was 50 μdm^3. Quality checks of the IC-analyses were

238 performed with both internal and external reference samples (Das et al., 2011). The analytical

239 detection limits obtained for the various ions, defined as twice the level of peak-to-peak

240 instrument noise, was 0.0001 μeq dm^{-3} for MSA. The overall analytical accuracy was better

241 than 1.5%.

242

2.3   Back-trajectories and meteorological data

For every hour during the ten years 2006 through 2015 three-dimensional back trajectories have been calculated arriving at 474 m at Mt. Zeppelin. The trajectories have been calculated backward for up to ten days using the HYSPLIT4 model (Draxler and Rolph, 2003) with meteorological data from the Global Data Assimilation System with one-degree resolution (GDAS1). Trajectories extending backwards for ten days are inaccurate at origin due to the trajectory uncertainty of 25-30% of its length, (Stohl, 1998). More information about the GDAS dataset can be found at Air Resources Laboratory (ARL), NOAA (http://ready.arl.noaa.gov), from which the meteorological data were downloaded.

During the analyzed time period meteorological records at the Mt. Zeppelin station are rather limited in quality and were frequently interrupted. There are no precipitation measurements and wind measurements are strongly influenced by the station building and by the local topography. In order to have an internally consistent, and unbroken meteorological record we utilized hourly meteorological parameters at trajectory arrival times as calculated by the HYSPLIT4 model. We emphasize that their accuracy depends on the quality of the meteorological model inside HYSPLIT4 and the accuracy and representativeness of the meteorological fields utilized by the model. Of the local meteorological record air temperature was considered the most reliable and thus explored in a comparison of trajectory calculated and modeled meteorological data. When comparing the 42600 contiguous hourly records from 2008-01-01 until 2012-11-10 the average ratio of measured and calculated temperatures is 0.98, with a coefficient of determination of 0.96. The utilized model parameters are listed in Table 1.

As an additional parameter we evaluated the vertical air movement of the trajectories during the last hour before arrival by subtracting the trajectory height one hour before arrival

276 at the arrival height of 474 meter. The resulting vertical displacement parameter, DZ, is given

277 in meters per hour. Positive values of DZ indicate a lifting of the air.

278 The most important missing meteorological information concerns the local cloud cover.

279 No direct recording was available of times during which the station was in clouds. The

280 closest available cloud instrument is a ceilometer operated by the Alfred Wegener Institute

281 (AWI) at their Koldewey Station in Ny-Ålesund, i.e. in the valley below Mt. Zeppelin, some

282 2.8 km of horizontal distance from the position of the mountain station. From the one-minute

283 records of the ceilometer we derived hourly values of the 25% percentile of cloud base, which

284 was used as an indicator for the Zeppelin station being in cloud. This ceilometer parameter is

285 listed as C25 in Table 1.

286 Precipitating clouds scavenge the planetary boundary layer and thus reduce the available

287 particle surface as condensation sink of particle precursors. As a consequence nucleation

288 from the gas phase may be facilitated (Tunved et al., 2013). As in Tunved et al. (2013) we

289 utilized the HYSPLIT-modeled precipitation along the back trajectories. Sums of

290 precipitation, (SP, see Table 1), were calculated along each back trajectory and will be

291 referred to as SP1 (during the last day), SP2 (during the last but one day), and SP5 (during

292 days three to five) before arrival at Mt. Zeppelin.

293

294

295 **2.4 Marine biological data**

296

297 The biologically active marginal ice zone is a major natural source of sulfur in the Arctic

298 summer atmosphere, (Leck and Persson, 1996b, a), and Wiedensohler et al. (1996), indicated

299 a potentially important role of dimethyl sulfide (DMS) in regional new particle formation.

300 DMS emissions from the sea have long been proposed to control new particle formation in the

301 marine boundary layer, (Charlson et al., 1987), which builds on DMS_{aq} being transported via

319 turbulence and diffusion to the sea-air interface, represented by the transfer velocity, which in

320 turn depends on sea-surface temperature, salinity, and wind speed, (Liss and Merlivat, 1986).

321 Once in the atmosphere DMS_g is photochemical oxidized via intermediates such as sulfuric

322 acid and methane sulfonic acid, (Ayers et al., 1996), which eventually leads to the formation

323 of aerosol $nssSO_4^{2-}$ and MSA. The products of the photochemical oxidation of DMS the ratio

324 MSA/ $nssSO_4^{2-}$ show a temperature dependence (Bates et al., 1990), favoring MSA in the cold

325 Arctic environment (Karl et al., 2007).

326 Dimethyl sulfide in the ocean (DMS_{aq}) is produced through the degradation of its algal

327 precursor dimethylsulfoniopropionate (DMSP) by microbial food webs, (Simó, 2001). At

328 high latitudes, total DMSP (DMSPt) and therefore DMS_{aq}, essentially follows the seasonal

329 cycle of phytoplankton biomass, (Lana et al., 2012). DMSPt is defined as the sum of

330 $DMSP_{dissolved}$ and $DMSP_{particulate}$ concentration. Yet, the amount of DMSPt per unit

331 phytoplankton biomass may vary depending on species composition and physiological state,

332 (Keller et al., 1989).

333 The dissolved organic carbon (DOC) concentrations in surface waters of the high Arctic

334 Ocean are up to ten times higher than in any other ocean basin and closer in range to DOC

335 levels reported for sea ice (Gao et al., 2012). A large fraction of DOC spontaneously

336 assembles into polymer gels: polysaccharide forming hydrated calcium bonded three-

337 dimensional networks to which other organic compounds, such as proteins and lipids, are

338 readily bound. The assembly and dispersion of the polysaccharide molecules can be affected

339 by environmental parameters, such as UV-B radiation (280-320nm) dispersing or inhibiting

340 gel formation, and/or pH and temperature inducing gel volume phase changes (swelling and

341 shrinkage). In the study of Orellana et al., (2011b), the swelling and shrinking of the

342 polysaccharide networks or polymer gels were also causally related by additions of nano to

343 micromolar levels of DMS and DMSP. High DMSP concentrations have also been measured

345   in the mucilage surrounding prymnesiophyte *Phaeocystis pouchetii* colonies in Arctic waters,

346   representing up to 25% of the total water column DMSP pool, (Matrai and Vernet, 1997).

347   The findings made by Orellana et al., (2011b) were in agreement with previous findings by

348   Orellana et al., (2011a) that high concentrations of DMSP and DMS are stored in the acidic

349   secretory vesicles of the *Phaeocystis* algae where DMSP is trapped within the condensed

350   polyanionic gel matrix until the secretory vesicles are triggered by environmental factors such

351   as temperature to release gels that undergo volume phase transition and expand at the higher

352   pH of seawater. Exocytosis of polymer gels accompanied by elevated DMS and DMSP

353   concentrations suggests the transport of these chemical compounds by the gel matrix.

354   Schoemann et al., (2005) report that *Phaeocystis antarctica* is particularly well adapted to low

355   temperatures, being more competitive than *P. pouchetii for temperatures between* -2 and

356   +2 °C. *Phaeocystis pouchetii*, however, appears to be better adapted to temperatures closer to

357   5 °C. In the Arctic a higher occurrence of the *Phaeocystis pouchetii* would be expected in the

358   northward advection of warm Atlantic water masses around Svalbard.

359   Here we estimated DMSPt at the sea surface using the algorithm described by Galí et al.

360   (2015). The DMSPt algorithm exploits the distinct relationship between DMSPt and

361   Chlorophyll-*a* depending on the light exposure regime of the phytoplankton community. The

362   light exposure regime is defined by the ratio between euphotic layer depth and mixed layer

363   depth (Z_{eu}/MLD). Additional predictor variables used are sea surface temperature (SST) and

364   particulate inorganic carbon (PIC), which is used in the algorithm as a proxy for

365   coccolitophores such as *Emiliania huxleyi*. During late bloom stages, the calcite plates that

366   cover coccolitophore cells (called coccoliths) detach and cause an increase in seawater

367   backscatter that invalidates satellite retrievals of Chlorophyll-*a*. Therefore, inclusion of PIC

368   in the algorithm as a proxy for DMSPt increases data coverage. Although the algorithm was

369   developed for the global ocean, validation results with in situ data indicate that it performs as

370   well or slightly better in Arctic and sub-Arctic waters.

371   The use of remotely sensed DMSPt as a proxy for marine DMSaq emission is a significant

372   improvement with respect to prior studies that used Chlorophyll-*a* (Becagli et al., 2016;

373   Zhang et al., 2015).   Yet, it is not ideal because (i) the ratios $DMS_{aq}/DMSPt$ in surface

374   seawater are variable, and tend to be higher in high solar irradiance and nutrient-poor

375   conditions typical of summer, (Galí and Simó, 2015), and (ii) even if DMSPt is a better proxy

376   for DMS_{aq}, the influence of meteorological and sea surface conditions (mainly wind speed

377   and SST) on the sea-air flux of DMS_{aq} is not taken into account.   Development is underway of

378   an algorithm for the retrieval of DMS_g concentrations in air and DMS fluxes.

379   The DMSPt algorithm was run for the 2006-2015 period using daily composites of the

380   Moderate Resolution Imaging Spectroradiometer on the Aqua satellite (MODIS-Aqua) at 4.64

381   km resolution (L3BIN, reprocessing R2014.0) downloaded from NASA's Ocean Color

382   website (http://oceancolor.gsfc.nasa.gov).   The MODIS variables used include Chlorophyll-*a*

383   concentration derived with the GSM algorithm, (Maritorena et al., 2002), PIC, nighttime SST

384   and Z_{eu}. MODIS nighttime SST was complemented with SST from the Advanced Very High

385   Resolution Radiometer (AVHRR, https://podaac.jpl.nasa.gov/AVHRR-Pathfinder) to increase

386   data availability.   MLD was obtained from the MIMOC climatology, (Schmidtko et al.,

387   2013), which was linearly interpolated from its original 0.5°x0.5° grid at monthly resolution

388   to the MODIS grid at daily resolution.

389   Satellite remote sensing of biological activity in surface waters requires ice-free and at

390   least part of the time cloud-free. The passive sensing methods of MODIS additionally require

391   a minimum of solar illumination of the scenes (i.e., solar zenith angle < 70°; (IOCCG, 2015)).

392   Consequently, the length of the satellite-observable period used to compute DMSPt means

393   shortens from all-year-round at latitudes <45° to approximately six months (the spring-

394   summer semester) at 80°N. In addition, the annual DMSPt map in Fig. 3 excludes all land and

395   ice covered regions.   In order to increase data coverage, daily DMSPt composites were binned

396   to five-day periods and a 46.4 km equal-area sinusoidal grid, (10x10 bins of the original pixel

397 size). The average distance between a trajectory point and the closest center of a MODIS

398 pixel is 18 km.

399   Following the same approach as with the ice data average DMSPt from ocean color data,

400 (OC), along each back trajectory were calculated and will be referred to as OC1 (the last day),

401 OC2 (the last but one day), and OC5 (days three to five) before arrival at Mt. Zeppelin. In

402 this procedure missing data were flagged as such, and were not taken into account.

403

404

405 **2.5   Ice data**

406

407 For the interpretation of events of new particle formation observed during the *Oden* cruises

408 information on pack ice extent under the air masses reaching the sampling points proved

409 crucial (Heintzenberg et al., 2015). Another motivation for utilizing ice data in the present

410 study is the fact that the Svalbard region experiences large seasonal changes in pack ice cover

411 which we expect to have strong effects on emissions of particles and their precursor gases.

412 Thus daily ice concentrations were taken from the NSIDC database (https://nsidc.org/data).

413 The irregularly shaped data gap around the pole caused by the inclination of satellite orbits

414 and instrument swath was filled with 100% cover. To each hourly position and data of the

415 back trajectories the ice information in the corresponding maps of ice concentrations were

416 added and displayed in Fig. 2. On average the closest pixel in the ice maps was about 12 km

417 off any trajectory point.

418   In the discussion of results we utilize the complement of ice cover, i.e., the amount of open

419 water because the marine biological processes of interest predominantly take place in the

420 open water, (Leck and Persson, 1996a). As integral parameters average open water, (OW),

421 percentages along each back trajectory were calculated and will be referred to as OW1 (the

422 last day*)*, OW2 (the last but one day), and OW5 (days three to five) before arrival at Mt.

423 Zeppelin. The most solid ice cover is seen in an area reaching from Northeastern edge of

424 Greenland via North Pole to Parry Island. A marginal ice zone extends along the east coast of

425 Greenland to Franz-Josef-Land, and the area between Svalbard and the latter island.

426

427

428 **2.6 ERA-Interim data of sea surface temperature**

429

430 Daily Sea Surface Temperature (SST) data for our study period (2006-2015) were

431 downloaded from the website of the European Centre for Medium-Range Weather Forecasts

432 (ECMWF). A description of the global atmospheric reanalysis, (ERA-Interim), has been

433 given by Dee et al. (2011), and a guide to the products and the download procedures can be

434 found at http://www.ecmwf.int/en/elibrary/8174-era-interim-archive-version-20. Briefly,

435 ERA-Interim is an assimilating model reanalysis of the global atmosphere and sea-surface

436 physical parameters covering the data-rich period since 1979. SST data were downloaded at a

437 resolution of approximately 0.56° and regridded onto the same 46 km equal-area sinusoidal

438 grid used for DMSP and cloud fraction, (see below). Ice-covered pixels were screened out

439 prior to the back-trajectory analysis. In the Arctic region, ERA-Interim has been shown to be

440 a top performer among a number of atmospheric reanalyses, (Lindsay et al., 2014).

441

442

443 **2.7 MODIS cloud fraction**

444

445 Persistent cloud cover limits PPP in Arctic and Sub-arctic seas, (Bélanger et al., 2013), and,

446 as mentioned above, irradiance at the sea surface, which is largely controlled by cloudiness,

447 influences $DMSP_{dissolved}$-to-DMS_{aq} conversion. Boundary layer clouds are known to be

448 additional controllers of the surface aerosol (Heintzenberg, 2012). In the summer Arctic low

449 level clouds and fogs are widespread (Warren and Hahn, 2002). Both scavenging and new

450 particle formation have been observed in connection with low clouds and fog passages

451 (Lannefors et al., 1983; Heintzenberg and Leck, 1994; Leck and Bigg, 1999; Heintzenberg et

452 al., 2006; Karl et al., 2013). Beyond the cloud base derived from the ceilometer we have no

453 other in situ local or regional cloud information. Thus, we utilize satellite-derived cloud

454 information.

455 Daily Level-3 global cloud fraction with one-degree resolution was downloaded from

456 NASA website (http://modis-atmos.gsfc.nasa.gov, Hubanks et al., 2015) and extracted for our

457 region of interest. Briefly, level 3 images correspond to the aggregation of all level 2 images

458 (1 km resolution) available within the one-degree resolution grid. For a given L2 scene, each

459 pixel is assigned a value of 1 (cloudy) or zero (clear sky), and then the individual scene values

460 are averaged over a 24-hour period. Note that a given pixel can be revisited up to six or seven

461 times in the course of a day at high latitudes. Finally, the daily composites were re-projected

462 to 46.4 km pixels to match the spatial resolution of DMSPt. The average distance between a

463 trajectory point and the closest MODIS pixel was 18 km.

464 The cloud fraction CF as well as other cloud properties from MODIS have been

465 extensively used, for instance to study the global spatial and temporal distribution of clouds

466 over the last decade (e.g., King et al., 2013). Several studies have also successfully

467 performed validation by comparison with in situ data (e.g., An and Wang, 2015) which

468 demonstrated the ability of the MODIS-aqua sensor to retrieve cloud cover.

469 Following the same approach as with the ice data and DMSPt, average cloud fractions,

470 (CF, see Table 1), along each back trajectory were calculated and will be referred to as CF1

471 (the last day), CF2 (the last but one day), and CF5 (days three to five) before arrival at Mt.

472 Zeppelin. Missing data are flagged as was done with DMSPt data.

473

474

3. Three approaches to identifying events of new particle formation

476

477 There are no definitive and no generally accepted methods to identify or predict NPF-events

478 in atmospheric time series of aerosol data. Thus, in the present study we explored different

479 approaches with varying degrees of complexity to identify such events. We emphasize that

480 none of these approaches explicitly is connected to diel cycles such as in Dal Maso et al.,

481 (2005) or makes any assumptions about the time of day during which new particle formation

482 occurs. Three objective search algorithms were written in FORTRAN to analyze the time

483 series of hourly records of aerosol parameters in search of new particle formation:

484 1. The simplest approach of upper percentiles (PCT-approach), assumes that NPF-events are

485   characterized by extremely high concentrations of small particles in terms of N25 (see

486   Table 1). The key parameter characterizing each PCT-event was the value of N25

487   averaged over a fixed number of hours, ($N25_{av}$), after the nominal start of an event, (see

488   below). With $N25_{av}$ also a nominal length of PCT-events was defined as the number of

489   hours after the start of an event by which N25 sank to less than half of $N25_{av}$.

490 2. The more specific approach of diameter growth (DGR-approach) builds on the temporal

491   development of the particle size distribution in terms of a systematic growth of the

492   diameter D50 (see section 4.1) to find the classical "Banana Type" of NPF-event,

493   (Kulmala et al., 2004). The key parameter characterizing each DGR-event was the average

494   growth of D50 during the nominal event length NUC, (see below). For this approach the

495   nominal length of events was reached when the running two-hour average growth fell

496   below the value one.

497 2. The most complex approach of multiple-size events, (MEV-approach), searches for events

498   with concurrent appearance of concentration increases in several size classes below 60 nm

499   diameter (Karl et al., 2013; Leck and Bigg, 2010). The key parameter characterizing each

500   MEV-event was the relative concentration increase averaged over the chosen size classes

501   below 60 nm during the nominal event length NUC, (see below). As with PCT-events a

502   nominal length of MEV-events was defined as the number of hours after the start of an

503   event by which N25 sank to less than half of $N25_{av}$.

504

505   Three time-related parameters were commonly defined for all three approaches:

506   1. Nominal NPF-event length, (NUC) was nine hours.

507   2. Pre-event periods, (PRENUC), from which increases in diameters or number

508   concentrations were calculated, were six hours.

509   3. Reference periods, (REF), before PRENUC and after NUC periods were defined in order

510   to compare event and pre-event data with non-event conditions. Each of these reference

511   periods had the length of half the sum of pre-event plus event time periods, making the

512   total reference time period of each event as long as that of the event itself.

513   Besides these common characteristic lengths individual fixed thresholds were chosen and

514   discussed below for each approach in order to generate at least 200 unique events per

515   approach, (see Table 2).

516   The aerosol data used to define the NPF-events were complemented by a large number of

517   environmental parameters. The primary temporal resolution of the environmental parameters

518   was between one minute (C25, cf. Table 1) and five days (DMSPt, cf. Table 1). C25 was

519   calculated as 25% percentile on an hourly basis. The parameters with resolutions higher than

520   an hour (OW, CF, and OC, cf. Table 1) were evaluated along the hourly back trajectories.

521   While this procedure yielded hourly varying results even of OW, CF, and OC it has to be kept

522   in mind that this hourly variability is the result of hourly resolved trajectories traversing the

523   grid; the low primary temporal resolutions of the OW, CF, OC, and chemical parameters

524   remain. For these slowly varying parameters the REF periods before and after the events

525   were extended to one day beyond the longest primary resolution, i.e., six days.

526   For two reasons the three search algorithms may yield temporarily redundant results, i.e.,

527   they may identify the same events. One, they go independently through the same time series

528   of aerosol data, possibly causing inter-approach redundancy. Two, each algorithm goes

529   through the time series hour by hour, thus allowing for temporal overlap of events found by

530   each approach, (intra-approach redundancy).

531   The three types of events were assumed to be mutually exclusive and potentially being

532   caused by different sets of conditions for new particle formation. Thus, a FORTRAN

533   procedure was developed to eliminate both intra and inter-approach redundancy while

534   maintaining a maximum of identified NPF-events. To remove intra-approach redundancy the

535   procedure identifies overlapping events within each approach. Of each ensemble of such

536   overlapping events the one with the strongest key parameter of the respective approach

537   (growth of D50, or concentration increases as defined above) is retained. Next, inter-

538   approach redundancy is addressed by the procedure. However, there is no unique solution to

539   the problem of the partly redundant three time series of events. In order to avoid any

540   preference of one or several types of events in the tests of inter-approach overlap pairs of

541   events of different approaches are chosen at random and compared for overlap. This random

542   comparison is done as often as the product of the number of events of the three approaches.

543   This rather time-consuming random test yields stable numbers of non-overlapping events

544   within less than one percent, irrespective of the order in which the events of the three

545   approaches were arranged for the test. By removing intra and inter-approach redundancy in

546   the first two steps of the procedure a number of time periods will be "freed". Consequently,

547   in a last step, the procedure tries to fill the "freed time periods" non-redundantly with events

548   of the three approaches that had been eliminated in the first two steps. Table 2 collects total

549   numbers and unique numbers of events for each approach. In the rest of the paper only non-

550   redundant events will be discussed. The total number of new particle formation events will

551   be shortened to TNPF.

3.1 The upper percentile of N25 (PCT-approach)

Events of new particle formation were identified by time periods in which N25 was consistently, i.e. on average for three hours, above a set threshold. With a threshold of the 93%-percentile (170 cm^{-3}) 4143 PCT-events were identified in the total data set, only 240 of which were unique because most of them overlapped with event or pre-event times of the other two approaches. Average N25 during these unique events was 330 cm^{-3} and the average length of events 4 ±0.9 h, (one standard deviation).

Fig. 4, (top), shows the average temporal development of the relative size distributions for the unique PCT-events as in the results in Karl et al. (2013), i.e. relative concentrations were formed by dividing the absolute number concentrations by the average total number during the six-hour pre-event time periods. The events are characterized by a nearly monomodal distribution around 20 nm that broadens somewhat around the nominal start of the events. During the last three hours before the events D50 decreased slightly and returned to the pre-event level during the nine NUC hours.

In connection with PCT-events average aerosol parameters NTO through N300 showed an average increase by a factor of 2.2 during PRENUC-periods, which was maintained on an average level of 1.5 during the events. The aerosol-chemical parameters Na$^+$, nssSO$_4^{-2}$, and MSA were on an average level of 20% of their reference value. The average environmental parameters indicate a strong increase by a factor of 14 in solar radiation and a lifting of cloud base before the events. During the events the level of solar radiation was still elevated by a factor of six above its reference value. As a consequence temperature at the station was up by 2 – 3 degrees. Precipitation 12 h before trajectory arrival time, (SP12) was a factor of five above reference levels for air arriving during NUC-periods, whereas SP35 to SP5D were below their respective reference levels. Cloud fractions were slightly raised 12 - 48 h before air arrival. Of the ocean parameters more open water was met by trajectories 12 to 24 before

580 their arrival with ocean temperatures 12 to 48 h before trajectory arrival having been up to
581 four degrees warmer than their respective reference values. On average DMSPt-parameters
582 OC24 through OC5D showed were raised by a factor of two above their reference value.

583   In Fig. 5, (left top panel), average trajectory height profiles during PRENUC and NUC-
584 periods are displayed. Widely varying vertical air mass paths occurred before and during
585 PCT-events. Median vertical trajectory paths during PRENUC and NUC times indicated air
586 coming from some 300 m above station level five days ago sinking to about one hundred
587 meters above station level during the last two days before arrival. The upper quartiles of the
588 PCT-height profiles point at strong subsidence before air mass arrival.

589   The right top panel in Fig. 5 maps average horizontal trajectory positions in 12 h steps in
590 months having at least ten PCT-events, i.e., May - September. Filled circles around the
591 trajectory positions comprise 95% of all events. The monthly average horizontal trajectory
592 direction during PCT-events mostly was from the northwest. In June and July the trajectories
593 reached farthest into the multiyear ice cover northeast of Greenland. Only during September
594 the back trajectories covered ice-free and marginal ice areas in the Fram Strait. We note that
595 the five-day back trajectories of PCT-events, (and of the other two approaches as well), stayed
596 within some 800 km of Mt. Zeppelin.

597

598

599   **3.2   The diameter growth (DGR) approach**

600

601 The DGR-approach to identify events of new particle formation builds on the classical
602 concept of particle growth through condensable vapors after an initial nucleation of sub-five
603 nanometer particles that cannot be observed with the available instrumentation, so called
604 "Banana-type" (Kulmala et al., 2004). The respective algorithm utilizes the parameter D50,
605 (see Table 1), and requires a growth of this diameter by at least a factor of 1.5 after the

606 nominal start of an event. With this threshold the algorithm searched through all 87646 hours

607 of the ten-year record and found 1199 DGR-events of new particle formation. After

608 eliminating cases of temporal overlap with the other two approaches 235 unique events of this

609 type remained, (see Table 2). Other or more DGR-events could have been found by

610 shortening the nominal nine NUC hours. For two reasons we refrained from discussing

611 shorter growth periods in the DGR-approach. Maintaining common-length NUC periods

612 facilitated the comparison of results of the three approaches. Furthermore, reducing the

613 growth period would also make PCT and DGR-events ever more similar.

614 Starting with an average value of D50 ≈ 16 nm at the nominal start of DGR-events an

615 average growth rate of 1.8 nmh^{-1} is derived, which is in the range of $1 – 2$ nmh^{-1} derived by

616 Ström et al. (2009) for new particle formation in the lower boundary over Ny-Ålesund,

617 Spitsbergen but considerably lower than the maximum growth rate of 3.6 nmh^{-1} reported by

618 Asmi et al. (2016) for July at the Siberian station Tiksi at the coast of the Laptev Sea. For

619 open ocean new particle formation events over the North Atlantic O'Dowd at al. (2010) report

620 a "typical growth rate" of 0.8 nmh^{-1}, whereas Ehn et al. (2010) give an average growth rate of

621 3 nmh^{-1}. The average length of DGR-events was 10 ±1 h, (one standard deviation).

622 The average temporal development of the relative number size distribution during DGR-

623 events is presented in Fig. 4, (center). After a decrease of the sub-50 nm diameter median

624 from about 25 to 16 nm during the six hours before the nominal start of the events D50

625 increases systematically during the following nine NUC hours with somewhat reduced growth

626 towards the end of the event.

627 During the PRENUC-periods particle number concentrations N300, and the condensation

628 sink, (CS), decreased relative to the reference periods before and after the events.

629 Subsequently, during the NUC periods the strongest increases was found for N60.

630 Environmental parameters around air mass arrival showed a strong lifting of cloud base,

631 (C25), and an extremely high increase in solar radiation, (by a factor of 11 during PRENUC

rev. 2017-2-18 10:48
Gelöscht: The

633 and by a factor of 60 during NUC periods). However, 12 h before air arrival precipitation had

634 been up by a factor of 2.5. Cloud fractions were down to about 70% of their reference values

635 24through 48 h before air arrival. Of the chemical aerosol parameters Na^+ and $nssSO_4^{-2}$

636 showed an increase of 2.6 and 2.3, respectively. OC12 and OC48 were slightly higher than

637 reference level before and during the events. Sea surface temperatures T24 were raised by

638 nearly one degree whereas earlier SST-values, (T36 – T5D), were up to one degree below

639 reference values.

640   Fig. 5, (left center panel), shows statistics of the vertical air movement before trajectory

641 arrival during DGR-events at Mt. Zeppelin covering a wide range of vertical movements

642 between 200 m and beyond 1500 m height. During the days when elevated DMSPt levels

643 were noted median trajectory heights were six to nine hundred meters. Median trajectories

644 during PRENUC times dipped down to the station level, (474 m a.s.l), about one day before

645 arrival, albeit lifted and subsided again shortly before arrival. Vertical trajectory pathways

646 will be discussed further in Section 4.2.

647   Monthly average trajectory positions and their variability in connection with DGR-events

648 are shown in Fig. 5, (center right panel). The months April through October had at least ten

649 DGR-events per month. As with PCT-events the general trajectory direction was from the

650 northwest, mostly staying for several days over the marginal ice zone between northeastern

651 Greenland and eastern Svalbard. During the earliest month of April with 14 DGR-events the

652 back trajectories reached farthest south into the ice-free parts of the Fram Strait.

653

654

655 **3.3   The Multiple-size approach (MEV)**

656

657 Leck and Bigg (2010) and Karl et al. (2013; 2012) discussed a type of new particle formation

658 that to date only has been reported from the summer Arctic. During these MEV-events high

659   ultrafine particle concentrations appear concurrently in a broad diameter range reaching from

660   under 10 to some 60 nm. We simulated this type in a search that required the concurrent

661   increase of NTO, N20, N40, and N60, (cf. Table 1), as averaged over the first three NUC

662   hours by a factor ≥ 1.6 over their respective averages during the six (PRENUC) hours. Over

663   the ten years of data 1191 such events of this type were identified, 266 of which remained

664   after removal of those overlapping with events of other approaches. During these unique

665   events the average concurrent concentration increase was 4.7 and the average length of the

666   events 12±0.8 h.

667   The concurrent appearance of high concentrations at many particle sizes below 60 nm

668   resembles the nocturnal NPF-events analyzed by Suni et al. (2008) in the Australian

669   Eucalyptus forest and simulated in subsequent chamber experiments (Ristovski et al., 2010;

670   Junninen et al., 2008). We emphasize though that the condensing vapors in the Australian

671   NPF-events originating from terrestrial biogenic emission are quite different from the

672   polymer gels implicated in the Arctic MEV-events and originating from the surface

673   microlayer of the ocean.

674   The bottom part of Fig. 4 shows the average temporal development of relative number size

675   distributions before and during MEV-events. The development before the nominal start of

676   MEV-events is more complex than during the PRENUC-periods of the first two types of

677   events. Intermittently a mode around seven nanometers shows up that broadens and becomes

678   more prominent about two hours before the nominal start of events. The major PRENUC-

679   mode around 25 nm also broadens and becomes more prominent towards NUC. A weak

680   mode exists during PRENUC around 120 nm and hardly any particles beyond 400 nm. D50

681   sinks from 25 to about 20 nm and stays below 25 nm through the MEV-events even though

682   number concentrations increase during the first NUC-hours by more than a factor of five.

683   During NUC-periods all particle number concentrations increased, on average by a factor

684   of 1.6. Average solar radiation also increased by about 90% above reference level during

685   NUC-periods. Of the chemical parameters $nssSO_4^{-2}$ showed an increase by a factor of three

686   during PRENUC and NUC-periods, and MSA a slight increase during PRENUC-periods. On

687   one hand, precipitation 12 h, and 36 to 48 h before trajectory arrival, (SP12, SP48), were

688   above reference levels for air arriving during PRENUC-periods. On the other hand, during

689   PRE, SP24, SP36, an SP5D indicated dry conditions during PRENUC and NUC-periods.

690   Only three to five days before air arrival slightly increased cloud fractions were noted. Sea

691   surface temperatures up to five days before trajectory arrival were on average about one

692   degree lower than their reference values. DMSPt parameters OC12 to OC36 were raised by

693   factors of 1.3 and 1.6 during PRENUC and NUC-periods, respectively.

694   Percentiles of vertical trajectory coordinates prior to and during MEV-events are displayed

695   in Fig. 5, (bottom left panel). During the events, and even stronger during the PRENUC

696   periods median trajectories had been below 500 m for more than four days. Furthermore, the

697   final air approach to Mt. Zeppelin mostly came from below the station level. Upper quartiles

698   of the vertical trajectory positions are substantially lower than with DGR-events. We note,

699   however, that a short excursion above station level occurred in the upper quartiles during the

700   last three hours before arrival.

701   The bottom right panel of Fig. 5 gives the monthly average trajectory positions and their

702   variability in connection with MEV-events. The months April through October had at least

703   ten MEV-events per month. As with the other approaches the general trajectory direction was

704   from the northwest, albeit with stronger swings towards the ice-free areas south of Svalbard

705   early and late in the season, (April, May, and September). Interestingly, the trajectories of the

706   11 MEV-events in October were directed nearly straight north from the North Pole.

707   Summarizing differences and commonalities among the results of the three approaches we

708   can state that the length of the events increases from four to ten and twelve, going from PCT

709   to MEV-events. PCT-events are characterized by lower-than-reference aerosol-chemical

710   parameters. Na^+ and $nssSO_4^{-2}$ show strong increases in the other two types of events: Na^+ in

711   connection with DGR-events and $nssSO_4^{-2}$ in connection with MEV-events. Both, PCT and

712   DGR-events exhibit strong increases in solar radiation. Precipitation before air arrival was

713   raised at varying times in connection with the three types of events. Cloudiness both

714   increased and decreased at varying times before air arrival with the three types of events.

715   Increased open water under the trajectories was strongest with DGR-events and least

716   important with MEV-events. Only in connection with PCT-events strongly raised sea surface

717   temperature were noted before trajectory arrival. DMSPt related ocean parameters were

718   raised to varying degrees and at varying times before all NPF-events, most strongly in

719   connection with PCT-events and least in connection with DGR-events.

720

721

722   **4. Discussion**

723

724   **4.1.   Environmental setting**

725

726   The discussion of the results on new particle formation in the Svalbard region builds on the

727   variability of new particle formation and related environmental parameters on scales of

728   months, and days. Fig. 1 gives an overview over the geographic areas which were covered by

729   one, two, and five-day back trajectories to Mt. Zeppelin during the ten years of the present

730   study covering the months March through October. This figure illustrates that air arriving at

731   Mt. Zeppelin during the ten summers of the present study came from widely varying regions

732   from the central ice-covered Arctic via the northern seas and northernmost Scandinavia to

733   Greenland. One-day back trajectories cover a roundish area from the central east coast of

734   Greenland via northern Scandinavia to Franz-Josef-Land, North Pole and back to the north

735   coast of Greenland. Excluding inner Greenland this area is widened by roughly 500 km by 2-

736   day back trajectories and by at least another 500 km by 5-day back trajectories reaching over

rev. 2017-2-18 10:48
Gelöscht: bot

rev. 2017-2-18 10:48
Gelöscht:

739   most of Greenland and the adjacent seas west of Greenland. This is a much wider region

740   from which air may reach Mt. Zeppelin as compared to sites in the inner Arctic as illustrated

741   in Fig. 2 of Heintzenberg et al. (2015).

742   On the path of trajectories to Mt. Zeppelin quite different ice conditions were met (see,

743   Fig. 2). On average North Atlantic open waters reached around West Spitsbergen all the way

744   to Nordaustlandet. Drift ice was passed over by trajectories along the whole east coast of

745   Greenland. One-day trajectories passed over the marginal ice zone from the Fram Strait to

746   Franz-Josef Land but also over more contiguous ice close to the North Pole. At times, with

747   five-day back trajectories, even the marginal ice regions of Baffin Bay and Beaufort Sea were

748   reached.

749   The long-term geographical distribution of DMSPt in Fig. 3 reflects the water conditions

750   for phytoplankton biomass around Svalbard. Directly at the coasts of Greenland and Eurasia

751   increased nutrient availability in coastal and shelf waters (due to continental run-off and

752   enhanced hydrodynamics) cause localized areas of high DMSPt values. The low DMSPt

753   values further out along the coast of Greenland are due to sea ice reaching through the Fram

754   Strait far south, (see Fig. 2). A prominent feature in the regional DMSPt distribution is the

755   tongue of high DMSPt, (intense blue color), and thus high phytoplankton biomass east of this

756   area, reaching from Spitsbergen to roughly Jan Mayen that lies within one-day back

757   trajectories. Northward-flowing Atlantic waters, carried by the West Spitsbergen Current,

758   and southward-flowing fresh surface waters from melting ice, and recirculated Atlantic

759   waters, carried by the East Greenland Current (Rudels et al., 2005) are meeting. The layering

760   created by water masses of different density stabilizes the water column and traps

761   phytoplankton cells at well-lit depths. If sufficient nutrients are available, this can lead to the

762   development of large phytoplankton blooms, which can result in high concentrations of

763   DMS_{aq}, (see Fig. 2 in Leck and Persson, 1996a).

764   In the ten-year average cloud fractions systematic differences in cloudiness appear.

765   Depending on transport pathways as identified by the back trajectories, cloudiness varies on

766   the way to Spitsbergen. The ice-covered areas, (cf. Fig. 2), from the east coast of Greenland

767   to Franz-Josef-Land exhibit somewhat lower cloud fractions than the ice-free regions

768   southwest to east of Spitsbergen.

769

770

771   **4.2   Seasonal variability**

772

773   Seasonal changes are discussed in terms of monthly averages taken over the ten-year study

774   period. As expected in Earth's polar regions the seasonal variability of all environmental

775   parameters is very high as exemplified by the solar flux, (SFL), and the air temperature,

776   (TEM), at Mt. Zeppelin in Fig. 6. Due to the seasonal change in cloudiness, (cf. Fig. 7), the

777   seasonal distribution of SFL is not quite symmetrical about midsummer but is skewed slightly

778   towards the cloud minimum in spring. The air temperature, however, does not peak before

779   July and has a broad shoulder into fall and winter. The first, and partly absolute maxima, of

780   the seasonal distributions of NPF-events in Fig. 6 coincide with that of the SFL but then drop

781   of more slowly towards fall than solar radiation. In particular, MEV-events do so and even

782   have their main maximum in August. The occurrence of all NPF-events drops off sharply in

783   October. Whereas May as the first month with larger numbers of events is dominated by

784   PCT-events, followed by DGR and then MEV-events, the contributions of the three NPF-

785   types are reversed in the last month with high NPF-numbers, i.e., September.

786   Fig. 6 clearly shows that the formation of new particles in the Svalbard region is not

787   controlled by the late winter-to-early-spring phenomenon of Arctic haze peaking with highest

788   sulfate-concentrations in March, (cf. Fig. 3 in Heintzenberg, 1989, and Fig. 6), which has a

789   minimum in the total number of NPF-events. This minimum is in contrast with the maximum

in new particle formation rates found by Croft et al. (2016a) with their global aerosol model. The high numbers of accumulation mode particles during the Arctic haze months in late winter and spring yield the annual maximum in condensation sink, (CS in Fig. 6), which could quench nucleation events and subsequent growth. Thus, even though photochemistry may produce significant amounts of nucleating material, the freshly formed particles will not grow to stable size before they are removed via either deposition or coagulation as discussed by Tunved et al. (2013) and others. An alternative explanation of the late onset of NPF-events in TNPF in spring lies in the marine biological processes not being activated nearby during the Arctic haze period yet, (Heintzenberg and Leck, 1994).

Fig. 7 collects the seasonal variation of environmental parameters as averaged along the back trajectories to Mt. Zeppelin. From their minimum in March-April open water conditions improve until September, after which the pack ice extent under the trajectories rapidly increases again. The widening open water areas are reflected in sea surface temperatures under the trajectories that increase until September before they drop off strongly in October. Consequently, because of its connection to marine biological activity DMSPt increases in the euphotic zone from first photosynthetic light in May until it evens out around July and drops off in October. Largest DMSPt values are reached in the vicinity of Svalbard, (cf. OC12 in July and August in Fig. 7), i.e. considerably later than MSA. The ending of DMSPt-curves in October is due to the lack of data not due to zero-DMSPt. Still, DMSPt concentrations are expected to be low at this time of the year at temperate to polar latitudes due to low phytoplankton biomass and low light exposure, (see Fig. 9 in Galí et al., 2015). In terms of the MODIS-derived cloud fraction cloudiness increases rapidly from its minimum in April and evens out on a plateau of 80 – 90% after July. The spring-minimum in cloudiness is confirmed by the maximum in cloud base as indicated by C25 in Fig. 7. This seasonal distribution of cloudiness does not correspond to the classical picture of near-surface cloudiness that exhibits near cloud-free conditions in winter and mostly overcast with Arctic

817   stratus and fogs during the summer months (Warren and Hahn, 2002; Huschke, 1969). We

818   explain the difference by the specific atmospheric pathways covered by the back trajectories

819   of the present study (cf. Fig. 1). Trajectory-averaged precipitation parameters (SP12-5D in

820   Fig. 7) have minima in the period April – May, from which they increase towards their

821   maxima in fall and winter.

822   The chemical aerosol information derived from the analyses of filters samples has a

823   relatively low temporal resolution of at least one day combined with frequent gaps of several

824   days in between samples. Thus, it cannot directly be related to the time periods of NPF-

825   events. The seasonal distribution of chemical tracers, however, yields important information

826   about new particle formation. Taken over the whole year $nssSO_4^{2-}$ in Fig. 6 is largely

827   anthropogenic, (Heintzenberg and Leck, 1994), and has its maximum during the peak of

828   Arctic haze in March and April and its minimum in August, which does not match any

829   seasonal distribution of NPF-events. We also plotted Na^+ in Fig. 6 as a tracer of the inorganic

830   marine aerosol components sea salt. Na^+ decreases from its winter maximum to its summer

831   minimum in June/July, again without similarity to the NPF-distributions. Instead, the

832   seasonal distribution of Na^+ rather closely follows that of the trajectory-derived wind speed

833   during the last hour before arrival, (not shown in the figure). Wind speed as driver for sea salt

834   production is a well established phenomenon (Blanchard and Woodcock, 1957). After a steep

835   rise in April MSA in Fig. 6 sharply peaks in May and then gradually drops off towards its

836   minimum in October, more gradually than reported for data taken from 1991 to 2004 by

837   Sharma et al. (2012) and earlier than reported by Heintzenberg and Leck (1994), both at the

838   same station. Our seasonal distribution of MSA most closely resembles that of SFL, in Fig. 6,

839   albeit with its peak in May a month earlier that SFL and more strongly skewed towards

840   spring. According to Leck and Persson (1996b) on average the concentrations of the marine

841   biogenic sulfur components, (DMS and MSA), fell with a decline rate of about 30% per week

842 approaching zero values in September explained by reduced ppp (Leck and Persson, (1996a),

843 (consistent with Becagli et al., 2016).

844 As MSA is the only measured aerosol component with exclusively marine biogenic

845 sources, we illustrate its seasonal distribution in greater detail in Fig. 8. In this figure MSA-

846 concentrations measured on Mt. Zeppelin have been extrapolated along 5-day back

847 trajectories, forming monthly average monthly maps of potential MSA-sources during the

848 biologically most active months of March through October.

849 Fig. 8 yields several pieces of information that are relevant to the issue of new particle

850 formation. Early in spring the biological aerosol sources are limited to the North Atlantic and

851 Norwegian Sea. In April the tongue of newly opened waters between Novaya Zemlya and

852 Franz-Josef-Land seemingly is beginning to become biologically active. In May this area

853 widens towards the Barents Sea while the North Atlantic also becomes more active, reaching

854 the Fram Strait. In August two wide potential source regions cover the region from Northern

855 Greenland to the northern end of Scandinavia and the region Barents to Kara Sea. In

856 September even the pack ice north of Svalbard becomes biologically active, (Leck and

857 Persson, 1996a), and shows potential MSA sources, in particular, north of the northern coast

858 of Greenland. Finally, the very weak potential MSA sources in October appear to be situated

859 mainly over the Kara Sea and over the North Atlantic.

860 How do these seasonal distributions compare to those of the NPF-events identified by the

861 three search-approaches defined in Section 3? To address this question we constrained the

862 average seasonal distribution of environmental parameters to those hours that had been

863 identified by the NPF-events of the three approaches. However, none of the individual

864 seasonal distributions of constrained environmental parameters follows closely any of the

865 NPF-events. In particular, the main MSA peak remains in May, thus one month earlier than

866 any peak of the NPF-occurrences. To elucidate further potential differences in the three types

867 of NPF-events we return to the discussion of vertical pathways of related back trajectories,

rev. 2017-2-18 10:48
Gelöscht: items

869   (see Fig. 5). In this figure all three types of NPF-events exhibit a wide range of vertical

870   trajectory paths. As we expect the regional sources of primary particles and particle

871   precursors to be at or near the surface we segregated the NPF-events into subpopulations with

872   back trajectories that remained a given time below 500 m, (roughly station level). In Fig. 9

873   we collected the results concerning the 93 NPF-events that occurred with trajectories under

874   the 500 m limit, i.e., roughly 12% of all events. The top panel shows that the related

875   trajectories not only stayed below 500 m through most of the last five days before arrival but

876   close to the surface until they started rising to the station level about 24 h before arrival. The

877   peak of the sum of event occurrences now coincided with the main MSA peak in May, (see

878   center panel in Fig. 9). For DGR-events the May-maximum was particularly strong whereas

879   the PCT-predominantly occurred in May and June and MEV-events remained clustered

880   around the later part of summer, possibly coupled to SST and DMSPt.

881   A number of environmental parameters indicated substantial deviations from their

882   respective reference values during the months with most frequent occurrence of this sub-

883   population of NPF-events. Strongest deviations were noted for precipitation that was elevated

884   above reference levels two to five days before trajectory arrival, most prominently for DGR-

885   events in May, (by a factor of six 36 h before trajectory arrival). Strong positive deviations in

886   aerosol-chemical parameters only occurred with Na^+ in PCT and MEV-events, indicating

887   relatively high wind speeds near sea surface in the related air masses. MSA was elevated up

888   to 50% above reference levels only during MEV-events. Elevated levels of DMSPt were

889   noted with all three types of NPF-formation, most prominently for DGR-events 12 to 36

890   hours before which DMSPt was increased by a factor up to 1.7 relative to reference levels.

891   The bottom panel of Fig. 9 gives average trajectory positions in 12 h steps for the months

892   May through September. The circles around the steps comprise 95% of all trajectories.

893   During all months the trajectories stayed in the ice-free and marginal ice zone between Fram

894   Strait and Eastern Svalbard as illustrated by average July ice cover for the ten study years,

898 (for average monthly ice covers cf. Fig. 8). In particular during the earliest and latest months

899 of May and September the trajectories swing farthest south over the open water south of

900 Svalbard. We note that the complementary sub-population of results with trajectories

901 remaining above station level did not yield results that differed strongly from those for the

902 whole population of back trajectories.

903 As a last step in the discussion of seasonal variations in new particle formation a model is

904 formulated that describes the average sum of NPF-events, (TNPF), as a function of three

905 parameters, two of which are directly measurable at the site. With the linear combination of

906 the solar flux, (SFL, Wm^{-2}), average sea surface temperature under back trajectories 36 to 48

907 hours before their arrival at the site, (T48, °C), and condensation sink, (CS, 10^5 s^{-1}):

908

909 $$TNPF = 0.57 \cdot SFL + 15.4 \cdot T48 - 0.69 \cdot CS$$

910

911 TNPF as shown in Fig. 10, can be described within an average deviation of 5% taken over the

912 major months with new particle formation, April - October. Any other of the sea surface

913 parameters describes TNPF less satisfactorily.

914

915

916

917

918 **4.3 Diurnal variability**

919

920 Average hourly occurrence of the three types of NPF-events is plotted in Fig. 11, (top). The

921 three approaches yield rather similar diel variations. From their minimum during the night

922 and early morning hours they reach their maximum occurrence between 12 and 16 h UTC in

923 the afternoon. One might expect the differences between the NPF-types to be due to the

925   requirement of the three types of NPF formation being mutually exclusive. However, this

926   constraint does not exclude that they occur at the same time of day, only that they occur at the

927   same time on the same day.

928   Over the continents new particle formation and growth events of the classical "Banana-

929   type" usually exhibit an increase in measurable precursors such as sulfuric acid shortly after

930   sunrise followed by the detection of increased numbers of nanometer-sized particles between

931   one and two hours later (Kulmala et al., 2004), who deduce a connection to photochemically

932   produced condensable vapors from this daily pattern. In the Svalbard region the sun is up all

933   day between mid-April and the end of August. Consequently we would expect the

934   photochemical production of condensable vapors to have a smaller diurnal amplitude than at

935   lower latitudes, which in turn should even out the diurnal pattern of NPF-events to some

936   degree. Despite the relatively small daily variations in solar elevations the solar flux on Mt.

937   Zeppelin varied on average by more than a factor of five during the sunlit days (see curve

938   SFL in Fig. 11, bottom). The daily maximum of SFL between 12 and 15 UTC coincides well

939   with the average diel change in N25 and NPF-occurrence. As expected in particle growth due

940   to condensable vapors after initial nucleation the daily maximum in N10 precedes that of N25

941   by a few hours.

942   The other process controlling the development of newly formed small particles is the

943   diurnal development of the planetary boundary layer, (Kulmala et al., 2004). We have no

944   data on the daily variation in boundary layer structure over or near the measurement site. The

945   ceilometer data yield the only high-resolution information with some connection to the

946   structure of the planetary boundary layer. During the summer months these data show a

947   consistent daily variation with a jump in most frequent hourly cloud base by about 100 m

948   from about 1570 m after 09 UTC with rather stable values following until 16 UTC, after

949   which cloud base decreases again to values comparable to the early morning hours. The

950   hourly medians of the vertical displacement parameter DZ, (see Fig. 11, bottom), provide a

clearer diurnal variation. While being negative throughout the day, i.e. indicating subsiding air during the last hour before arrival at Mt. Zeppelin, DZ indicates the weakest subsidence in early afternoon. We interpret diurnal variation in cloud base and DZ as indicative of local clearing and convection during the day that may be conducive to photochemical processes and mixing in the boundary layer, both of which would be enhancing new particle formation.

5. Summary and conclusions

Three different types of events of new particle formation, (NPF), were identified through objective search algorithms formulated for the present study. The first and simplest algorithm utilizes short-term increases in particle concentrations below 25 nm, (PCT-events). The second one builds on the growth of the sub-50 nm diameter-median, (DGR-events), and is most closely related to the classical "banana-type" of events, (Kulmala et al., 2004) involving the presence of photochemically generated DMS oxidation precursors. The third and most complex, so-called multiple-size approach to identifying NPF-events builds on the hypothesis of Leck and Bigg (2010), suggesting the concurrent production of polymer gel particles at several sizes below about 60 nm, (MEV-events).

With these algorithms NPF-events were identified in a ten-year record of hourly number-size distributions taken at the research station on Mt. Zeppelin, Spitsbergen. As a first and general conclusion we can state that NPF-events are a summer phenomenon and not related to Arctic haze, which is a late winter-to-early spring event. The seasonal distribution of the available information on cloudiness does not suggest any direct connection with NPF-formation. The MODIS derived cloud fraction generally is very high (70 – 90%) and rather evenly distributed over the Svalbard region during the months with high frequencies of NPF-events. As already reported in Tunved et al. (2013), NPF-events appear to be somewhat

rev. 2017-2-18 10:48
Gelöscht: Conclusions

rev. 2017-2-18 10:48
Gelöscht: (2013)

979   sensitive to the available data on precipitation derived from the trajectory model, in particular

980   when constrained to cases with back trajectories staying below 500 m. In this subpopulation

981   of NPF-events DGR-events show the strongest change in precipitation parameters in

982   connection with new particle formation.

983   The seasonal distribution of solar flux suggests some photochemical control that may

984   affect marine biological processes generating particle precursors and/or atmospheric

985   photochemical processes that generate condensable vapors from precursor gases. Whereas

986   the seasonal distribution of the biogenic MSA follows that of the solar flux it peaks before the

987   maxima in NPF-occurrence. For PCT-events, and more distinctly so for DGR-events, this

988   one-month delay disappears in the subpopulation with back trajectories staying below 500 m.

989   MEV-events, however, maintain their peak occurrence later in summer and early fall.

990   With the limited information on particle size, composition, particle precursors, and

991   environmental conditions no definitive statements can be made about the processes leading to

992   the formation of new particles in the Svalbard region. A host of findings, however, point to

993   varying and rather complex marine biological source processes. The potential source regions

994   for all types of new particle formation appear to be restricted to the marginal ice and open

995   water areas between Northeastern Greenland and Eastern Svalbard. During earliest and latest

996   months with high numbers of NPF-events the back trajectories reach farther south into the

997   open waters of the North Atlantic. Depending on conditions yet to be clarified new particle

998   formation may become visible as short bursts of particles around 20 nm, (PCT-events), longer

999   events involving condensation growth, (DGR-events), or extended events with elevated

1000   concentrations of particles at several sizes below 100 nm, (MEV-events). The seasonal

1001   distribution of NPF-events peaks later than that of MSA and, DGR and in particular of MEV-

1002   events reach into late summer and early fall with much open, warm, and DMSPt-rich waters

1003   around Svalbard, promoting the production of *Phaeocystis pouchetii* together with polymer

1004   gels. Consequently, a simple model to describe the seasonal distribution of the total number

1005   of NPF-events can be based on solar flux, and sea surface temperature, representing

1006   environmental conditions for marine biological activity, and condensation sink, controlling

1007   the balance between new particle nucleation and their condensational growth. Based on the

1008   sparse knowledge about the seasonal cycle of gel-forming marine microorganisms and their

1009   controlling factors we hypothesize that the seasonal distribution of DGR and more so MEV-

1010   events reflect the seasonal cycle of the gel-forming phytoplankton.

1011   Despite the rather small diel changes expected during the summer Arctic there is a

1012   significant diurnal variation in aerosol and environmental parameters. Diurnal distributions

1013   of particle numbers below ten, (N10), and below 25 nm, (N25) follow that of the solar flux

1014   rather closely with a maximum between 14 and 16 UTC with the maximum of N10 occurring

1015   a few hours before that of N25. This delay in maxima may be caused by a slow particle

1016   growth due to photochemically produced condensable vapors. With a peak around noon

1017   MEV-events show the earliest daily peak occurrence with PCT and DGR-events peaking

1018   between 15 and 17 h, more closely to the maximum solar flux. Considering the diurnal

1019   variation in vertical trajectory displacement, (DZ), the early daily maximum in MEV-

1020   occurrence may be simply controlled by boundary layer dynamics.

1021   With the large database of ten years of aerosol data on Mt. Zeppelin enriched by

1022   environmental atmospheric and marine data occurrences, pathways and potential source areas

1023   of different types of new particle formation in the Svalbard region were elucidated by the

1024   present study. More process related information about new particle formation would require

1025   dedicated mechanistic experiments with more detailed information on particle precursors,

1026   ultrafine particles, and boundary layer mixing processes. DGR and MEV-types of new

1027   particle formation seem to be more closely related to near-surface processes. Thus, a low-

1028   level site such as the reopened Station Nord, (Nguyen et al., 2016), would be more suitable

1029   for related mechanistic experiments. Station Nord has the additional advantage of being close

1030   to the potential source regions of DGR and MEV-events identified by the present study.

Acknowledgements

The back trajectories created through the local use of the HYSPLIT4 model developed, maintained and generously distributed by the Air Resources Laboratory of NOAA were a backbone of the present study. We are very grateful for the ceilometer data provided by the Alfred-Wegener- Institute in Bremerhaven/Potsdam and to NSIDC for their providing daily Arctic sea ice data. Complementing our own chemical analyses of Mt. Zeppelin filter data, sodium and sulfate results were taken from the EBAS database at the Norwegian Institute for Air Research (http://ebas.nilu.no), for which we are indebted to Anne-Gunn Hjellbrekke and Wenche Aas. We thank the NASA Ocean Biology Distributed Active Archive Center (OB.DAAC) for access to MODIS datasets. We are indebted to Yafang Cheng and Zhibin Wang for providing the algorithm for calculating the condensation sink. MG acknowledges the receipt of a Beatriu de Pinós post-doctoral fellowship funded by the Generalitat de Catalunya. Long-term funding oft he DMPS measurements was provided by the Swedish Environmental Protection Agency (Naturvårdsverket). We also thank Norwegian Polar Institute for substantial support oft the field operation on Mt. Zeppelin.

Literature

Agarwal, J. K., and Sem, G. J.: Continuous flow, single-particle-counting condensation nucleus counter, J. Aerosol Sci., 11, 343-357, 1980.

An, N., and Wang, K.: A Comparison of MODIS-Derived Cloud Fraction with Surface Observations at Five SURFRAD Sites, J. Appl. Meteor. Clim., 54, 1009-1020, 2015.

Asmi, E., Kondratyev, V., Brus, D., Laurila, T., Lihavainen, H., Backman, J., Vakkari, V., Aurela, M., Hatakka, J., Viisanen, Y., Uttal, T., Ivakhov, V., and Makshtas, A.: Aerosol size distribution seasonal characteristics measured in Tiksi, Russian Arctic, Atmos. Chem. Phys., 16, 1271-1287, 10.5194/acp-16-1271-2016, 2016.

Ayers, G. P., Cainey, J. M., Granek, H., and Leck, C.: Dimethylsulfide oxidation and the ratio of methansulfonate to non sea-salt sulfate in the marine aerosol, J. Atmos. Chem., 25, 307-325, 1996.

Bates, T. S., Johnson, J. E., Quinn, P. K., Goldan, P. D., Kuster, W. C., Covert, D. C., and Hahn, C. J.: The biogeochemical sulfur cycle in the marine boundary layer over the Northeast Pacific Ocean, J. Atmos. Chem., 10, 59-81, 1990.

Becagli, S., Lazzara, L., Marchese, C., Dayan, U., Ascanius, S. E., Cacciani, M., Caiazzo, L., Di Biagio, C., Di Iorio, T., di Sarra, A., Eriksen, P., Fani, F., Giardi, F., Meloni, D., Muscari, G., Pace, G., Severi, M., Traversi, R., and Udisti, R.: Relationships linking primary production, sea ice melting, and biogenic aerosol in the Arctic, Atmos. Environ., 136, 1-15, http://dx.doi.org/10.1016/j.atmosenv.2016.04.002, 2016.

Beine, H. J., Argentini, S., Maurizi, A., Mastrantonio, G., and Viola, A.: The local wind field at Ny-Ålesund and the Zeppelin mountain at Svalbard, Meteorol. Atmos. Phys., 78, 107–113, 2001.

Bélanger, S., Babin, M., and Tremblay, J.-É.: Increasing cloudiness in Arctic damps the increase in phytoplankton primary production due to sea ice receding, Biogeosciences, doi:10.5194/bg-5110-4087-2013, 2013.

Blanchard, D. C., and Woodcock, A. H.: Bubble formation and modification in the sea and its meteorological significance, Tellus, 9, 145-158, 1957.

Browse, J., Carslaw, K. S., Mann, G. W., Birch, C. E., Arnold, S. R., and Leck, C.: The complex response of Arctic aerosol to sea-ice retreat, Atmos. Chem. Phys., 14, 7543-7557, 10.5194/acp-14-7543-2014, 2014.

Charlson, R. J., Lovelock, J. E., Andreae, M. O., and Warren, S. G.: Oceanic phytoplankton, atmospheric sulphur, cloud albedo and climate, Nature, 326, 655-661, 1987.

1087 Croft, B., Martin, R. V., Leaitch, W. R., Tunved, P., Breider, T. J., D'Andrea, S. D., and
1088   Pierce, J. R.: Processes controlling the annual cycle of Arctic aerosol number and size
1089   distributions, Atmos. Chem. Phys., 16, 3665-3682, 10.5194/acp-16-3665-2016, 2016a.
1090 Croft, B., Wentworth, G. R., Martin, R. V., Leaitch, W. R., Murphy, J. G., Murphy, B. N.,
1091   Kodros, J. K., Abbatt, J. P. D., and Pierce, J. R.: Contribution of Arctic seabird-colony
1092   ammonia to atmospheric particles and cloud-albedo radiative effect, Nature
1093   Communications, 7, 13444, 10.1038/ncomms13444
1094 http://www.nature.com/articles/ncomms13444 - supplementary-information, 2016b.
1095 Dal Maso, M., Kulmala, M., Riipinen, I., Wagner, R., Hussein, T., Aalto, P. P., and Lehtinen,
1096   K. E. J.: Formation and growth of fresh atmospheric aerosols: eight years of aerosol
1097   size distribution data from SMEAR II, Hyytiälä, Finland, Bor. Env. Res., 10, 323-336,
1098   2005.
1099 Das, R., Granat, L., Leck, C., Praveen, P. S., and Rodhe, H.: Chemical composition of
1100   rainwater at Maldives Climate Observatory at Hanimaadhoo (MCOH), Atmos. Chem.
1101   Phys., 11, 3743-3755, 10.5194/acp-11-3743-2011, 2011.
1102 Dee, D. P., Uppala, S. M., Simmons, A. J., Berrisford, P., Poli, P., Kobayashi, S., and
1103   Bechtold, P.: The ERA‐Interim reanalysis: Configuration and performance of the
1104   data assimilation system, Q. J. Roy. Meteorol. Soc., 137, 553-597, 2011.
1105 Draxler, R., and Rolph, G.: HYSPLIT (HYbrid Single-Particle Lagrangian Integrated
1106   Trajectory) Model access via NOAA ARL READY, NOAA Air Resources
1107   Laboratory, Silver Spring, MD, 2003.
1108 Ehn, M., Vuollekoski, H., Petäjä, T., Kerminen, V.-M., Vana, M., Aalto, P., de Leeuw, G.,
1109   Ceburnis, D., Dupuy, R., O'Dowd, C. D., and Kulmala, M.: Growth rates during
1110   coastal and marine new particle formation in western Ireland, J. Geophys. Res., 115,
1111   n/a-n/a, 10.1029/2010JD014292, 2010.
1112 Flyger, H., and Heidam, N. Z.: Ground level measurements of the summer tropospheric
1113   aerosol in Northern Greenland, J. Aerosol Sci., 9, 157-168, 1978.
1114 Galí, M., Devred, E., Levasseur, M., Royer, S.-J., and Babin, M.: A remote sensing algorithm
1115   for planktonic dimethylsulfoniopropionate (DMSP) and an analysis of global patterns,
1116   Remote Sens. Environ., 171, 171-184, http://dx.doi.org/10.1016/j.rse.2015.10.012,
1117   2015.
1118 Galí, M., and Simó, R.: A meta‐analysis of oceanic DMS and DMSP cycling processes:
1119   Disentangling the summer paradox, Global Biochem. Cycles, 29, 496-515, 2015.

1120   Gao, Q., Leck, C., Rauschenberg, C., and Matrai, P. A.: On the chemical dynamics of
1121   extracellular polysaccharides in the high Arctic surface microlayer, Ocean Sci.
1122   Discuss., 9, 215–259, 2012.

1123   Heintzenberg, J., Bischof, W., Odh, S.-Å., and Moberg, B.: An investigation of possible sites
1124   for a background monitoring station in the European Arctic., International
1125   Meteorological Institute in Stockholm, Department of Meteorology, Stockholm
1126   University, Stockholm, Report Nr. AP-22, 74 pp, 1983.

1127   Heintzenberg, J., and Larssen, S.: SO_2 and SO_4 in the Arctic: Interpretation of observations at
1128   three Norwegian Arctic-subArctic stations, Tellus, 35B, 255-265, 1983.

1129   Heintzenberg, J.: Arctic haze: air pollution in polar regions, AMBIO, 18, 50-55, 1989.

1130   Heintzenberg, J., and Leck, C.: Seasonal variation of the atmospheric aerosol near the top of
1131   the marine boundary layer over Spitsbergen related to the Arctic sulphur cycle, Tellus,
1132   46B, 52-67, 1994.

1133   Heintzenberg, J., Leck, C., Birmili, W., Wehner, B., Tjernström, M., and Wiedensohler, A.:
1134   Aerosol number-size distributions during clear and fog periods in the summer high
1135   Arctic: 1991, 1996, and 2001, Tellus, 58B, 41-50, 2006.

1136   Heintzenberg, J., Wehner, B., and Birmili, W.: "How to find bananas in the atmospheric
1137   aerosol" New approach for analyzing atmospheric nucleation and growth events,
1138   Tellus B, 59, 273-282, 2007.

1139   Heintzenberg, J.: The aerosol-cloud-climate conundrum, IJGW, 4, 219-241, 2012.

1140   Heintzenberg, J., Leck, C., and Tunved, P.: Potential source regions and processes of aerosol
1141   in the summer Arctic, Atmos. Chem. Phys., 15, 6487-6502, 10.5194/acp-15-6487-
1142   2015, 2015.

1143   Held, A., Brooks, I. M., Leck, C., and Tjernström, M.: On the potential contribution of open
1144   lead particle emissions to the central Arctic aerosol concentration, Atmos. Chem.
1145   Phys., 11, 3093-3105, 10.5194/acp-11-3093-2011, 2011a.

1146   Held, A., Orsini, D. A., Vaattovaara, P., Tjernström, M., and Leck, C.: Near-surface profiles
1147   of aerosol number concentration and temperature over the Arctic Ocean, Atmos.
1148   Meas. Tech., 4, 1603–1616, 2011b.

1149   Hubanks, P., Platnick, S., King, M., and Ridgway, B.: MODIS Atmosphere L3 Gridded
1150   Product Algorithm Theoretical Basis, Document (ATBD) and Users Guide, 2015.

1151   Huschke, R. E.: Arctic cloud statistics from "air calibrated" surface weather observations,
1152   Rand Corporation Memo. RM 6173-PR, 79 pp, 1969.

IOCCG: Ocean Colour Remote Sensing in Polar Seas, Report 16, Eds. Babin, M., Arrigo, K., Bélanger, S. and Forget, M.-H., 129 pp, 2015.

Jaenicke, R., and Schütz, L.: Arctic aerosols in surface air, Idöjaras, 86, 235-241, 1982.

Junge, C. E.: Air chemistry and Radioactivity, Academic Press, New York and London, 382 pp., 1963.

Junninen, H., Hulkkonen, M., Riipinen, I., Nieminen, T., Hirsikko, A., Suni, T., Boy, M., Lee, S.-H., Vana, M., Tammet, H., Kerminen, V.-M., and Kulmala, M.: Observations on nocturnal growth of atmospheric clusters, Tellus B, 60, 365-371, 2008.

Karl, M., Gross, A., Leck, C., and Pirjola, L.: Intercomparison of dimethylsulfide oxidation mechanisms for the marine boundary layer: Gaseous and particulate sulfur constituents, J. Geophys. Res., 112, D15304, 10.1029/2006JD007914, 2007.

Karl, M., Leck, C., Gross, A., and Pirjola, L.: A Study of New Particle Formation in the Marine Boundary Layer Over the Central Arctic Ocean using a Flexible Multicomponent Aerosol Dynamic Model, Tellus, 64B, doi:http://dx.doi.org/10.3402/tellusb.v3464i3400.17158, 2012.

Karl, M., Leck, C., Coz, E., and Heintzenberg, J.: Marine nanogels as a source of atmospheric nanoparticles in the high Arctic, Geophys. Res. Lett., 40, 3738–3743, DOI: 10.1002/grl.50661, 2013.

Keene, W. C., Pszenny, A. A. P., Galloway, J. N., and Hawley, M. E.: Sea-salt corrections and interpretation of constituent ratios in marine precipitation, J. Geophys. Res., 91, 6647-6658, 1986.

Keller, M. D., Bellows, W. K., and Guillard, R. R. L.: A survey of dimethylsulfide production in 12 classes of marine phytoplankton, in: Biogenic sulfur in the environment, edited by: E.S. Saltzman, and Cooper, W. J., American Chemical Society, Washington, D, 167–182, 1989.

King, M. D., Platnick, S., Menzel, W. P., Ackerman, S. A., and Hubanks, P. A.: Spatial and temporal distribution of clouds observed by MODIS onboard the Terra and Aqua satellites, IEEE Trans. Geosci. Remote Sens., 51, 3826–3852, 2013.

Knutson, E. O., and Whitby, K. T.: Accurate Measurement of Aerosol Electrical Mobility Moments, J. Aerosol Sci., 6, 453-460, 1975a.

Knutson, E. O., and Whitby, K. T.: Aerosol classification by electric mobility: apparatus, theory, and applications, J. Aerosol Sci., 6, 443-451, 1975b.

Kulmala, M., Dal Maso, M., Mäkelä, J. M., Pirjola, L., Väkevä, M., Aalto, P. P., Miikkulainen, P., Hämeri, K., and O'Dowd, C. D.: On the formation, growth and composition of nucleation mode particles, Tellus, 53B, 479-490, 2001.

Kulmala, M., Vehkamäkia, H., Petäjä, T., Dal Maso, M., Lauri, A., Kerminen, V.-M., Birmili, W., and McMurry, P. H.: Formation and growth rates of ultrafine atmospheric particles: a review of observations, J. Aerosol Sci., 35, 143-176, 2004.

Lana, A., Simó, R., Vallina, S. M., and Dachs, J.: Re-examination of global emerging patterns of ocean DMS concentration, Biogeochem., 110, 173-182, 2012.

Lannefors, H., Heintzenberg, J., and Hansson, H.-C.: A comprehensive study of physical and chemical parameters of the Arctic summer aerosol; results from the Swedish expedition Ymer-80, Tellus, 35B, 40-54, 1983.

Leck, C., and Persson, C.: The central Arctic Ocean as a source of dimethyl sulfide: Seasonal variability in relation to biological activity, Tellus, 48B, 156-177, 1996a.

Leck, C., and Persson, C.: Seasonal and short-term variability in dimethyl sulfide, sulfur dioxide and biogenic sulfur and sea salt aerosol particles in the arctic marine boundary layer, during summer and autumn, Tellus, 48B, 272-299, 1996b.

Leck, C., and Bigg, E. K.: Aerosol production over remote marine areas - A new route, Geophys. Res. Lett., 23, 3577-3581, 1999.

Leck, C., and Bigg, E. K.: New particle formation of marine biological origin, Aerosol Sci. Technol., 44, 570-577, 2010.

Leck, C., Gao, Q., Mashayekhy Rad, F., and Nilsson, U.: Size-resolved atmospheric particulate polysaccharides in the high summer Arctic, Atmos. Chem. Phys., 13, 12573-12588, 10.5194/acp-13-12573-2013, 2013.

Lindsay, R., Wensnahan, M., Schweiger, A., and Zhang, J.: Evaluation of seven different atmospheric reanalysis products in the Arctic, J. Clim., 27, 2588-2606, 2014.

Liss, P. S., and Merlivat, L.: Air-sea gas exchange rates: Introduction and synthesis, in: The Role of Air-Sea Exchange in Geochemical Cycling, edited by: Buat-Menard, P., Reidel, Norwell, MS, 113-127, 1986.

Maritorena, S., Siegel, D. A., and Peterson, A. R.: Optimization of a semianalytical ocean color model for global-scale applications, Appl. Opt., 41.15, 2705-2714, 2002.

Matrai, P. A., and Vernet, M.: Dynamics of the vernal bloom in the marginal ice zone of the Barents Sea: Dimethyl sulfide and dimethylsulfoniopropionate budgets, Journal of Geophysical Research: Oceans, 102, 22965-22979, 10.1029/96JC03870, 1997.

1225 Nguyen, Q. T., Glasius, M., Sørensen, L. L., Jensen, B., Skov, H., Birmili, W., Wiedensohler,
1226 A., Kristensson, A., Nøjgaard, J. K., and Massling, A.: Seasonal variation of
1227 atmospheric particle number concentrations, new particle formation and atmospheric
1228 oxidation capacity at the high Arctic site Villum Research Station, Station Nord,
1229 Atmos. Chem. Phys., 16, 11319–11336, 10.5194/acp-2016-205, 2016.

1230 Norman, A. L., Barrie, L. A., Toom-Sauntry, D., Sirois, A., Krouse, H. R., Li, S. M., and
1231 Sharma, S.: Sources of aerosol sulphate at Alert: Apportionment using stable isotopes,
1232 J. Geophys. Res., 104, 11619-11631, 1999.

1233 O'Dowd, C., Monahan, C., and Dall'Osto, M.: On the occurrence of open ocean particle
1234 production and growth events, Geophys. Res. Lett., 37, L19805,
1235 doi:19810.11029/12010GL044679, 2010.

1236 Orellana, M. V., Matrai, P. A., Janer, M., and Rauschenberg, C. D.:
1237 Dimethylsulfoniopropionate storage in *Phaecystis* (Prymnesiophyceae) secretory
1238 vesicles J. Phycol., 47, 112-117, 10.1111/j.1529-8817.2010.00936.x, 2011a.

1239 Orellana, M. V., Matrai, P. A., Leck, C., Rauschenberg, C. D., Lee, A. M., and Coz, E.:
1240 Marine microgels as a source of cloud condensation nuclei in the high Arctic, PNAS,
1241 108, 13612–13617, 2011b.

1242 Pirjola, L., Kulmala, M., Wilck, M., Bischoff, A., Stratmann, F., and Otto, E.: Formation of
1243 sulphuric acid aerosols and cloud condensation nuclei: An expression for significant
1244 nucleation and model comparison, J. Aerosol Sci., 30, 1079-1094, 1999.

1245 Polissar, A. V., Hopke, P. K., Paatero, P., Kaufman, Y. J., Hall, D. K., Bodhaine, B. A.,
1246 Dutton, E. G., and Harris, J. M.: The aerosol at Barrow, Alaska: long-term trends and
1247 source locations, Atmos. Environ., 33, 2441-2458, 1999.

1248 Rahn, K. A., and Shaw, G. E.: Particulate air pollution in the Arctic: Large-scale occurence
1249 and meteorological controls, in: Atmospheric Aerosols and Nuclei, edited by: Roddy,
1250 F., and O'Connor, T. C., Dept. of Physics, University College, Galway, Ireland 21-27
1251 Sept., 223-227, 1977.

1252 Ristovski, Z. D., Suni, T., Kulmala, M., Boy, M., Meyer, N. K., Duplissy, J., Turnipseed, A.,
1253 Morawska, L., and Baltensperger, U.: The role of sulphates and organic vapours in
1254 growth of newly formed particles in a eucalypt forest, Atmos. Chem. Phys., 10, 2919-
1255 2926, 10.5194/acp-10-2919-2010, 2010.

1256 Rudels, B., Björk, G., Nilsson, J., Winsor, P., Lake, I., and Nohr, C.: The interaction between
1257 waters from the Arctic Ocean and the Nordic Seas north of Fram Strait and along the

East Greenland Current: results from the Arctic Ocean-02 Oden expedition, Journal of Marine Systems, 55, 1-30, 2005.

Schmidtko, S., Johnson, G. C., and Lyman, J. M.: MIMOC: A global monthly isopycnal upper-ocean climatology with mixed layers, Journal of Geophysical Research: Oceans, 118, 1658-1672, 10.1002/jgrc.20122, 2013.

Schoemann, V., Becquevort, S., Stefels, J., Rousseau, V., and Lancelot, C.: Phaeocystis blooms in the global ocean and their controlling mechanisms: a review, Journal of Sea Research, 53, 43-66, http://dx.doi.org/10.1016/j.seares.2004.01.008, 2005.

Sharma, S., Chan, E., Ishizawa, M., Toom-Sauntry, D., Gong, S. L., Li, S. M., Tarasick, D. W., Leaitch, W. R., Norman, A., Quinn, P. K., Bates, T. S., Levasseur, M., Barrie, L. A., and Maenhaut, W.: Influence of transport and ocean ice extent on biogenic aerosol sulfur in the Arctic atmosphere, J. Geophys. Res., 117, D12209, 10.1029/2011JD017074, 2012.

Simó, R.: Production of atmospheric sulfur by oceanic plankton: biogeochemical, ecological and evolutionary links, Trends in Ecology & Evolution, 16, 287-294, 2001.

Stohl, A.: Computations, accuracy and applications of trajectories - A review and bibliography, Atmos. Environ., 32, 947-966, 1998.

Ström, J., Engvall, A.-C., Delbart, F., Krejci, R., and Treffeisen, R.: On small particles in the Arctic summer boundary layer: observations at two different heights near Ny-Ålesund, Svalbard, Tellus B - Chemical and Physical Meteorology, 61, 473-482, 2009.

Suni, T., Kulmala, M., Hirsikko, A., Bergman, T., Laakso, L., Aalto, P. P., Leuning, R., Cleugh, H., Zegelin, S., Hughes, D., van Gorsel, E., Kitchen, M., Vana, M., Hõrrak, U., Mirme, S., Mirme, A., Sevanto, S., Twining, J., and Tadros, C.: Formation and characteristics of ions and charged aerosol particles in a native Australian Eucalypt forest, Atmos. Chem. Phys., 8, 129-139, 10.5194/acp-8-129-2008, 2008.

Tunved, P., Ström, J., and Krejci, R.: Arctic aerosol life cycle: linking aerosol size distributions observed between 2000 and 2010 with air mass transport and precipitation at Zeppelin station, Ny-Ålesund, Svalbard, Atmos. Chem. Phys., 13, 3643–3660, 10.5194/acpd-12-29967-2012, 2013.

Warren, S. G., and Hahn, C. J.: Cloud climatology, in: Encyclopedia of Atmospheric Sciences, edited by: Holton, J. R., Pyle, J., and Curry, J. A., Academic Press, London, UK, 476-483, 2002.

1290 Wiedensohler, A., Covert, D., Swietlicki, E., Aalto, P., Heintzenberg, J., and Leck, C.:
1291   Occurrence of an ultrafine particle mode less than 20 nm in diameter in the marine
1292   boundary layer of the Arctic summer and autumn, Tellus, 48B, 213-222, 1996.
1293 Willis, M. D., Burkart, J., Thomas, J. L., Köllner, F., Schneider, J., Bozem, H., Hoor, P. M.,
1294   Aliabadi, A. A., Schulz, H., Herber, A. B., Leaitch, W. R., and Abbatt, J. P. D.:
1295   Growth of nucleation mode particles in the summertime Arctic: a case study, Atmos.
1296   Chem. Phys. Discuss., 2016, 1-31, 10.5194/acp-2016-256, 2016.
1297 Zhang, M., Chen, L., Xu, G., Lin, Q., and Liang, M.: Linking Phytoplankton Activity in
1298   Polynyas and Sulfur Aerosols over Zhongshan Station, East Antarctica, J. Atmos. Sci.,
1299   72, 4629-4642, 2015.
1300
1301
1302

1303

Parameter	TR (h)	Explanation
C25	1 min	25% percentile of cloud base from AWI ceilometer (m)
CF12, 24, 36, 48, 5D	24	Average MODIS cloud fraction during the last 12h, 24h, 36, 48h, and days 3-5 before trajectory arrival
D50	1	Number-median diameter of particles < 50 nm diameter
CS	1	Condensation sink (s^{-1})
DZ	1	Vertical trajectory displacement (m h^{-1}) during the last hour before arrival
MSA	≥1 day	Methane sulfonate (nmolm^{-3})
N10	1	Number concentration of particles up to 10 nm (>2010, cm^{-3})
N20	1	Number concentration between 10 and 20 nm (cm^{-3})
N25	1	Number concentration of particles up to 25 nm (cm^{-3})
N40	1	Number concentration between 20 and 40 nm (cm^{-3})
N60	1	Number concentration between 40 and 60 nm (cm^{-3})
N100	1	Number concentration between 60 and 100 nm (cm^{-3})
N300	1	Number concentration between 100 and 300 nm (cm^{-3})
Na	≥1 day	Sodium concentrations (nmolm^{-3})
NCO	1	Number concentration of particles > 300 nm (cm^{-3})
nssSO$_4^{2-}$	≥1 day	Non-sea salt sulfate concentrations (nmolm^{-3})
NTO	1	Number concentration of particles ≥ 10 nm, cm^{-3})
OC12, 24, 36, 48, 5D	120	Average MODIS DMSPt (nmol) during the last 12h, 24h, 36, 48h, and days 3-5 before trajectory arrival
OW12, 24, 36, 48, 5D	24	Average open water (%) during the last 12h, 24h, 36, 48h, and days 3-5 before trajectory arrival
PRE	1	Trajectory precipitation (mm) at arrival
RH	1	Trajectory relative humidity (%) at arrival
SFL	1	Solar flux at trajectory arrival (Wm^{-2})
SP12, 24, 36, 48, 5D	1	Accumulated precipitation (mm) during the last 12h, 24h, 36, 48h, and days 3-5 before trajectory arrival
T12, 24, 36, 48, 5D	24	Average sea surface temperature (C) during the last 12h, 24h, 36, 48h, and days 3-5 before trajectory arrival
TEM	1	Trajectory temperature (C) at arrival
WDR	1	Trajectory wind direction (°) during the last hour before arrival
WSP	1	Trajectory wind speed (m sec^{-1}) during the last hour before arrival

1304

1305   Table 1 Aerosol, atmospheric, and ocean parameters utilized in the present study.

1306   DMSPt = Total dimethylsulfoniopropionate in surface ocean waters. TR = temporal

1307   resolution in which the respective data were available. All parameter explanations

1308   starting with "Trajectory" refer to parameters calculated by HYSPLIT4 at each

1309   trajectory step.

1310

1311

1312

1313

1314

1315

1316

1317

1318

Approach	Acronym	Criteria and thresholds	Total number of events	Number of unique events	% of total number of data hours
Percentiles	PCT	N25 >93%-percentile	4143	240	1
Diameter-growth	DGR	D50-Growth >1.5	1199	235	3
Multi-size growth	MEV	Multi-growth >1.6	1191	266	4
Sum			6533	741	

1319

1320 Table 2 Total and unique number of events of new particle formation identified by the three

1321   approaches to identify NPF-events, and percent of all data hours covered by unique

1322   events.

1323
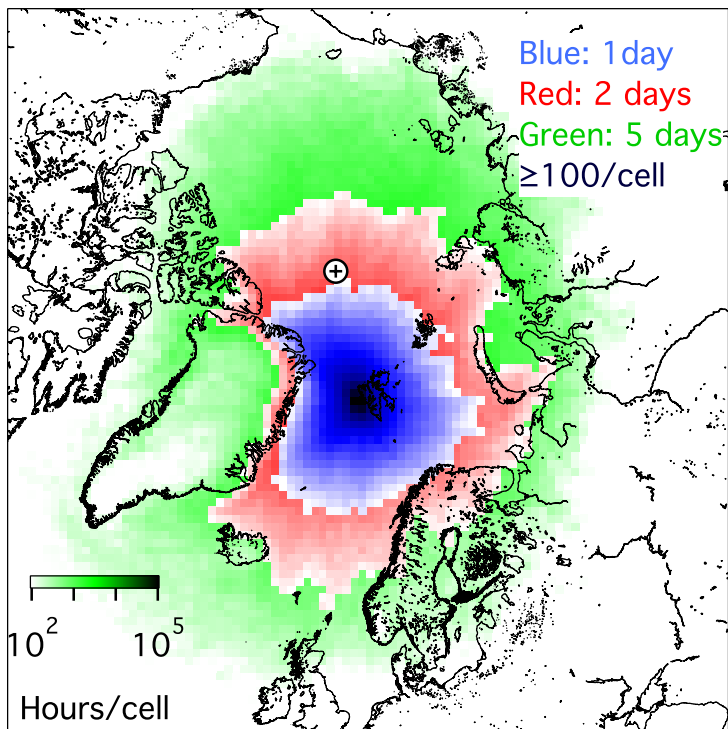
Fig. 1 Map of the regional distribution of 5-day (green), 2-day (red), and 1-day (blue) hourly back trajectories to Mt. Zeppelin during the months March through October of the years 2006 - 2015. Black symbol: North Pole. The colored areas are covered with at least 100 trajectory hours per geocell and the color saturation corresponds to the number of trajectory hours per grid cell on a log-scale.
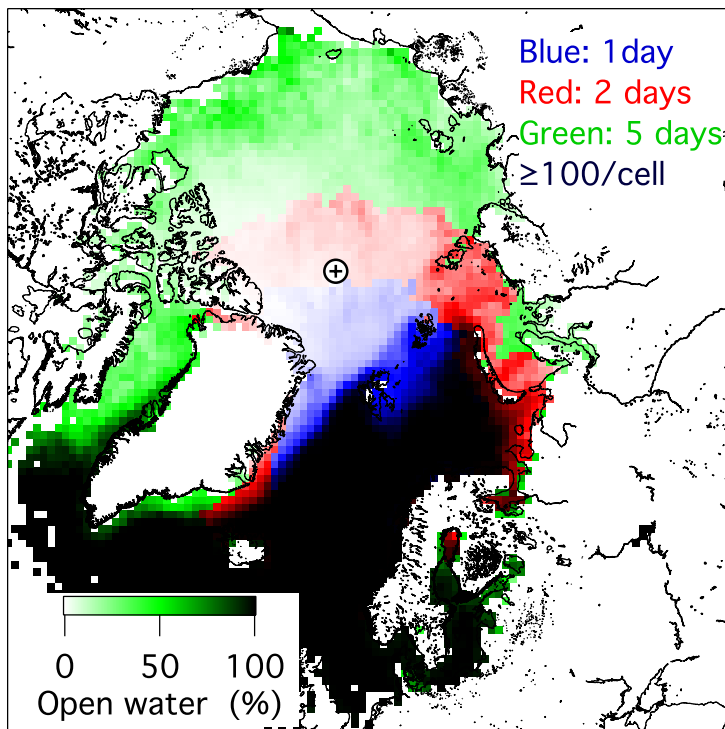
Fig. 2   Map of the regional distribution of open water under 87648 5-day (green), 2-day
(red), and 1-day (blue) hourly back trajectories to Mt. Zeppelin during the during the
months March through October of the years 2006-2015. Black symbol: North Pole.
The areas are covered with at least 100 trajectory hours concurrent with data values
per geocell.
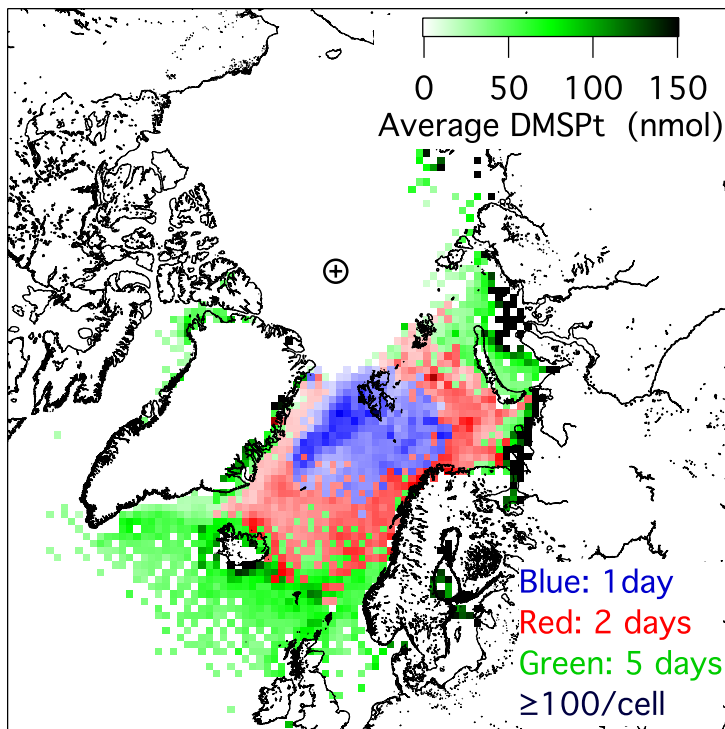
1339

1340   Fig. 3   Map of the regional distribution of DMSPt along 87648 5-day (green), 2-day (red),

1341   and 1-day (blue) hourly back trajectories to Mt. Zeppelin during the during the

1342   months March through October of the years 2006-2015. Black symbol: North Pole.

1343   The relative color scale holds for all colors. The areas are covered with at least 100

1344   trajectory hours with data values per geocell.

1345
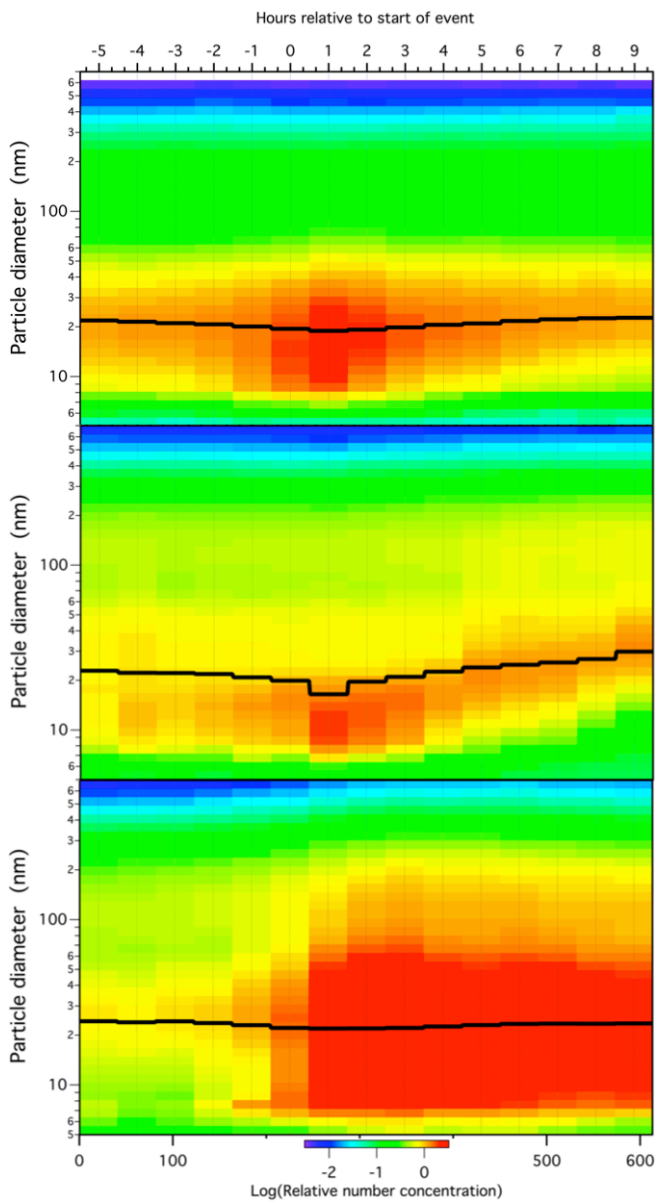
Fig.4   Average temporal development of the relative number size distribution before and
during NPF-events identified by the three approaches. The black curve gives the
median sub-50-nm particle diameter D50 during the events.   Top: PCT-events;
center: DGR-events; bottom: MEV-events.
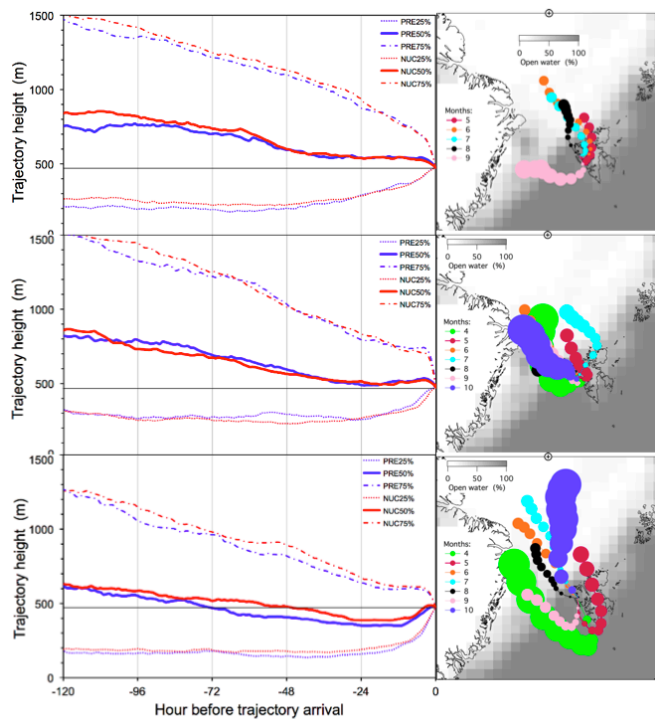
1352

1353   Fig. 5   Left panels: Median back trajectory height profiles (m) during the six pre-event

1354   hours (full line in blue, PRENUC) and during the nine DGR-event hours (full line in

1355   red, NUC). 25% and 75% percentiles are shown as dotted, and dash-dotted lines,

1356   respectively. Top: PCT-events; center: DGR-events; bottom: MEV-events. The thin

1357   horizontal line marks the station level.

1358   Right panels: Average monthly trajectory positions in 12 h steps for the months April

1359   though October. Only months with at least 10 NPF-events are shown. The circles

1360   comprise 95% of all trajectories at any trajectory step. The underlying grey-scale

1361   map indicates July ice cover averaged over the years 2006 – 2015

1362
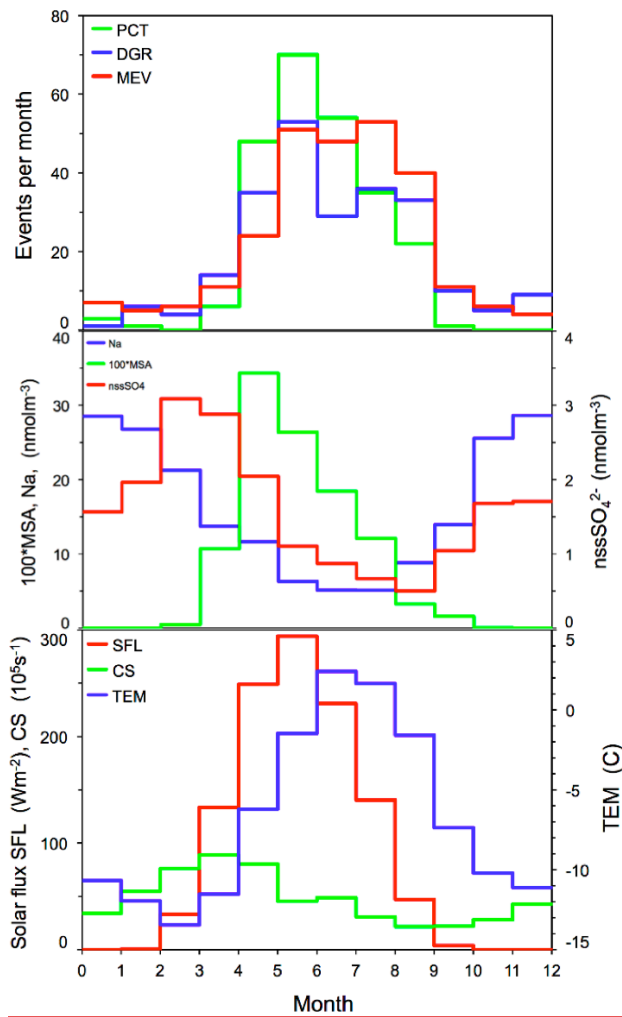
Fig. 6   Top: Monthly numbers of new particle formation events according to the three approaches, summed up over the whole period of ten years. PCT: Upper percentile of N25; DGR: Diameter growth; MEV: Multiple size events.

Center: Average seasonal distribution of particle composition in nmolm^{-3}. Na = sodium, nssSO4 = nssSO$_4^{2-}$, MSA = Methane sulfonate times 100.

Bottom: Monthly average solar flux (SFL, red, Wm^{-2}), and temperature (TEM, blue °C), and condensation sink, (CS, 10^5s^{-1}), at Mt. Zeppelin, Spitsbergen.

1373
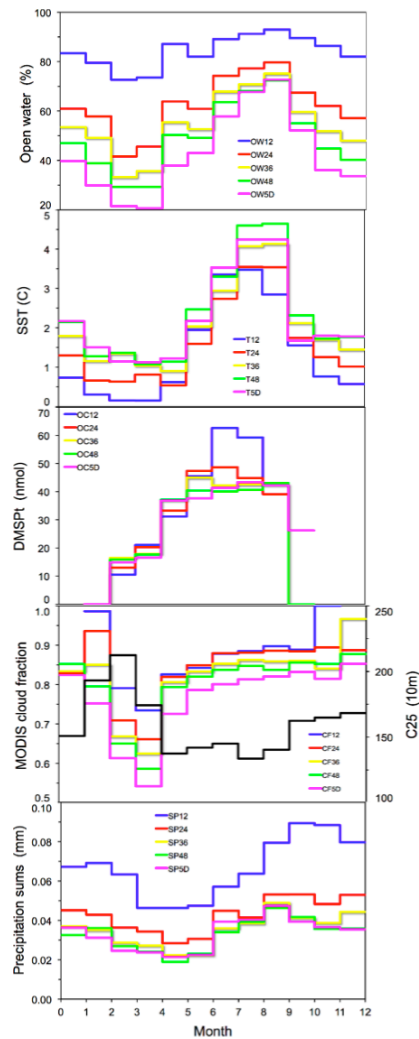
1374

1375 Fig. 7   Monthly averages of environmental parameters averaged along back trajectories to

1376   Mt. Zeppelin. From top to bottom: OW12-5D: Open water in % during last 12, 24,

1377   36, and 48h, and days 3-5 before trajectory arrival at Mt. Zeppelin. T12-5D: Same

1378   for sea surface temperature in °C. OC12-5D: Same for DMSPt in nmol in surface

1379   waters.   CF12-5D: Same for MODIS cloud fraction.   SP12-5D: Same for

1380   precipitation sums in mm. C25 = 25%-percentile of cloud base in decameter.

1381
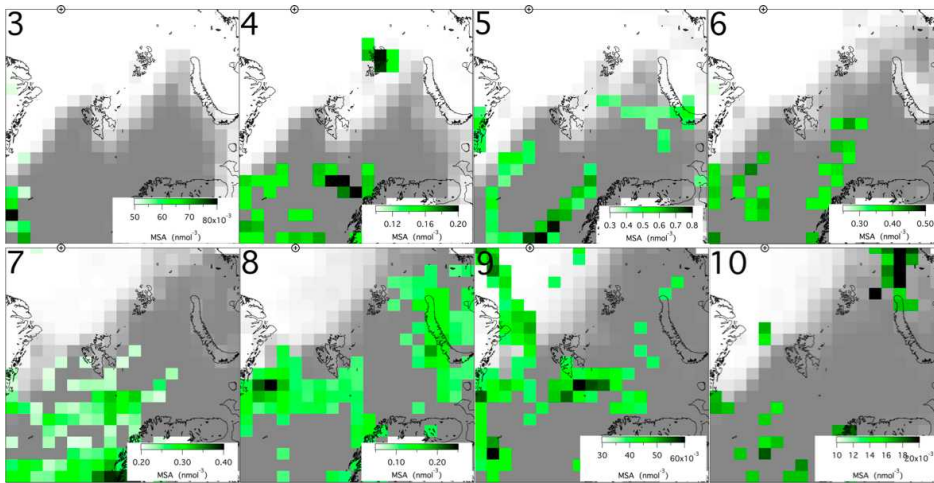
Fig. 8   Average monthly distribution of methane sulfonic acid, (MSA, nmolm^{-3}), during the months March – October of the years 2006 – 2015, constructed from MSA-concentrations measured on Mt. Zeppelin, which were extrapolated along 5-day back trajectories.   Average open water percentages during the respective months are indicated as white (0% open water) to dark grey (100% open water) areas.   The position of the North Pole is marked as cross in circle on the upper border of the maps.
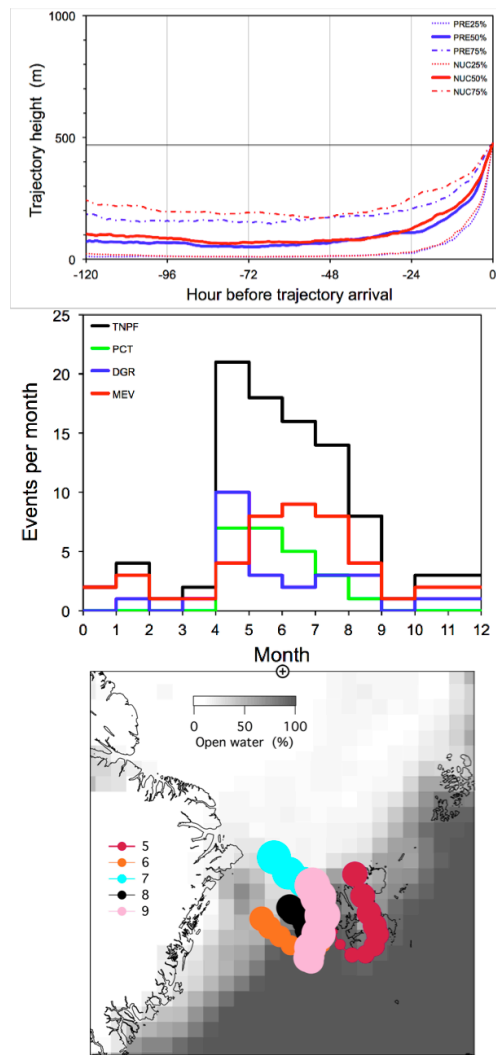
1391

Fig. 9   Characteristics of the subpopulation of 93 NPF-events with back trajectories that
stayed below 500 m for five days before arrival. Top: Statistics of related vertical
trajectory coordinates as in Fig. 5. Center: Average monthly occurrence of PCT,
DGR, and MEV-events, summed up over the whole period of ten years. Bottom:
Related average monthly trajectory positions in 12 h steps for the months May
through September. The circles comprise 95% of all trajectories at any trajectory

1399   step. The underlying grey-scale map indicates July ice cover averaged over 2006 –

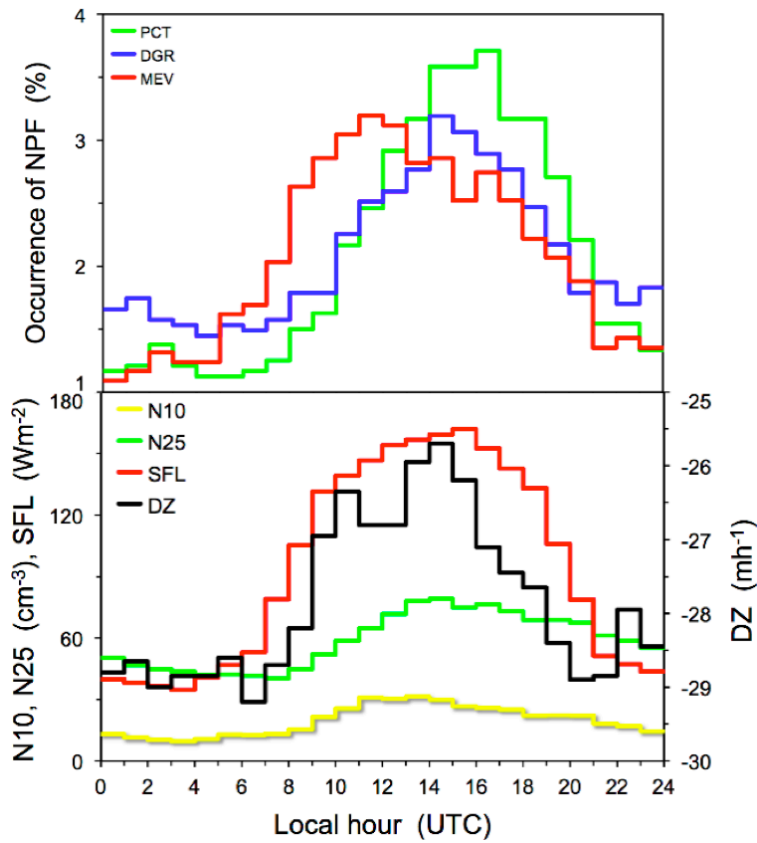1400   2015.

1401
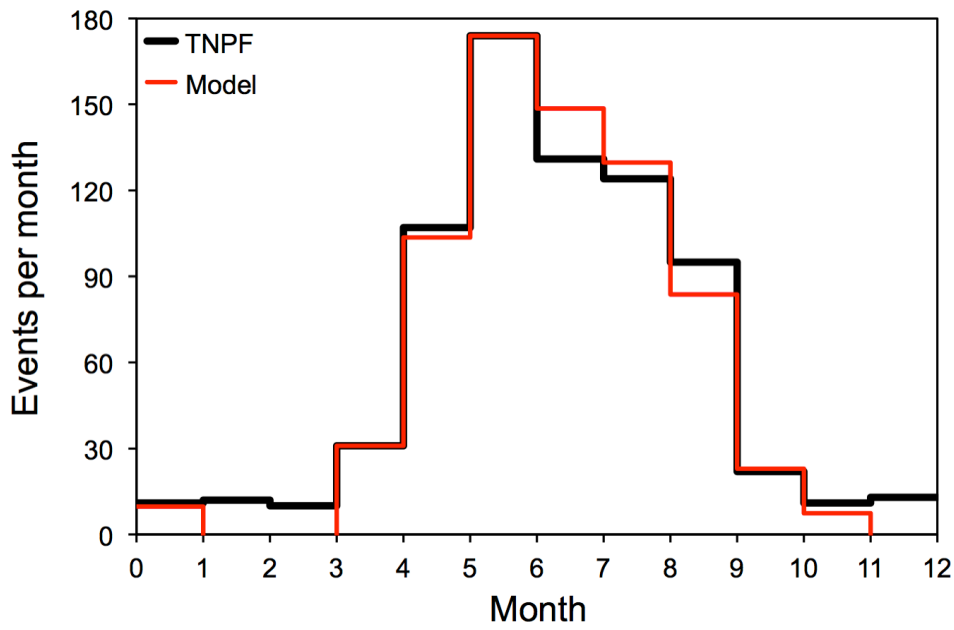
1402

1403   Fig. 10   Average monthly sums of NPF-events due to the three types of new particle

1404   formation, (TNPF, black), summed up over the whole period of ten years. Red:

1405   Three-parameter model to describe TNPF.

1406

1408

Fig. 11 Top: Relative average diurnal occurrence of the three types NPF-events. PCT:
Upper percentile of N25; DGR: Diameter growth; MEV: Multiple size events.
Bottom: Average diurnal variation of the HYSPLIT-modeled solar flux (SFL, Wm^{-2}),
the integral particle concentrations N10, and N25 in cm^{-3}, and of the vertical
displacement parameter (DZ, mh^{-1}). N10 is based on data of the years 2011 – 2015
whereas the other parameters are based on data of the years 2006 – 2015.